DPWA Winners 2023

TABLE OF CONTENT

PIANC De Paepe-Willems Award 2023 – Shared 1st Place

SYNTHETICALLY GENERATING TRAFFIC SCENARIOS FOR SIMULATION-BASED CONTAINER TERMINAL PLANNING

MARVIN KASTNER*, OLE GRASSE

Institute of Maritime Logistics,
Hamburg University of Technology (TUHH),
Hamburg, Germany

*Corresponding author: Marvin Kastner;
marvin.kastner@tuhh.de

Keywords: Container Terminal; Terminal Planning; Economic Traffic Forecast; Simulation Study; Synthetic Data; Traffic Scenario Generation

Mots-clés: Terminal à conteneurs; planification du terminal; prévision économique du trafic; étude de simulation; données synthétiques; génération de scénarios de trafic

1 CONTEXT AND MOTIVATION

Planning a container terminal involves many interrelated activities to ensure that the constructed terminal actually meets the expectations of the shareholders and stakeholders. As one of the first steps, the expected vessel fleet mix and expected cargo flows in an economic region are forecast for the next decades; in the scope of a subsequent analysis, it is then decided how to position the terminal in the market [Port Planning and Construction Committee, 2001]. The container terminal operator (or a port planner taking their perspective) needs to decide which cargo flows they try to attract to operate profitably. Based on the cargo flows that are expected to be routed through the terminal, the quay side, land side, and yard area are laid out [Wiese, Suhl & Kliewer, 2011]. At each of the interfaces (typically serving deep sea vessels, feeders, barges, trains, and/or trucks), typically short waiting times and high productivity are required. The yard area serves as a buffer between the discharging of a container from one vehicle and its loading onto another vehicle. The required yard capacity is then estimated based on the expected container volume p.a. and the expected container dwell time. In other words, the expected cargo flows and their characteristics are crucial when planning container terminals.

The first drafts of the quay side, land side, and yard area of the container terminal are often based on rough calculations using expected annual figures and average values [Chu & Huang, 2005]. Each draft might differ in terms of its layout or operating system, e.g. for transporting laden containers straddle carriers, rail-mounted gantry cranes and automated guided vehicles, or rubber-tired gantry cranes and tractor/trailer units are commonly used. Simulation comes into play once more specific questions arise and expected terminal key performance indicators are required [Kastner, Lange & Jahn, 2020]. Such questions could be 'How are terminal operations affected by supply chain disturbances?' or 'Can the terminal reach a certain berth productivity when two deep sea vessels are simultaneously served?' By constructing a digital twin of each terminal draft and experimenting with it, the stakeholders and shareholders gain first insights. These then support the decision making processes during the planning phase. In this context, the abstract long-term traffic forecasts need to materialise in concrete traffic scenarios consisting of virtual deep sea vessels, feeders, barges, trucks, and/or trains. These vehicles arrive at the digital twin of the terminal, request some or all containers to be discharged and some to be loaded before they depart again. Such traffic scenarios need to be created automatically and fast so that the digital twins can be thoroughly tested before selecting one of the drafts to be realised.

Whenever a simulation study is executed that covers the container handling processes at a terminal, inevitably at some point a traffic scenario is generated. Somehow, the vehicles and containers must enter and leave the container terminal. The data generation is often fully integrated into the simulation model. Hartmann (2004) has taken a different approach. He generates traffic scenarios by means of a separate software. Based on assumptions and random distributions, complex scenarios are generated. The data is then exported in a tabular format digestible by a simulation model. The same concept of separate scenario generation is further elaborated by Kastner, Grasse & Jahn (2022) who programmed an adjusted version of the algorithm in Python and shared the implementation online under a free license. The software is called 'ConFlowGen' and is invoked via an application programming interface. This allows the user to adjust the assumptions and distributions to their needs. To the best knowledge of the authors, this is currently the only freely accessible tool for traffic scenario generation at container terminals. But is it a suitable tool to support terminal planners?

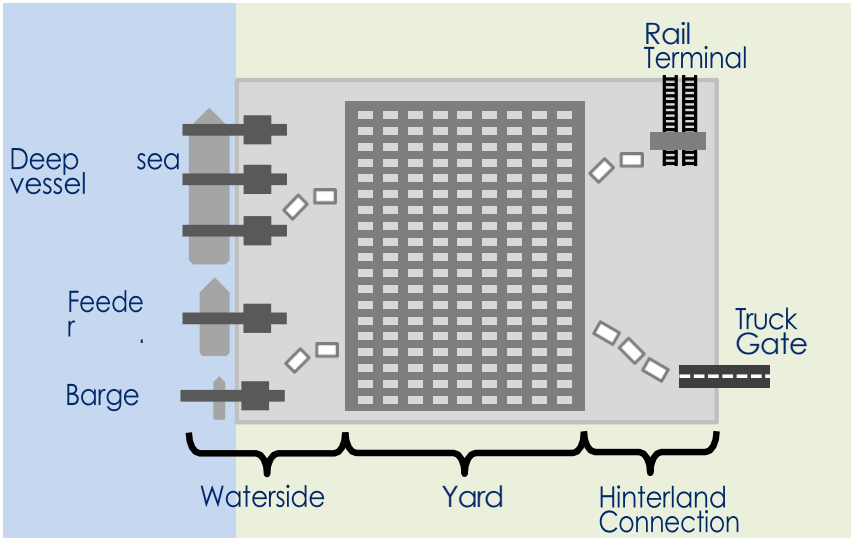

Figure 1: A container terminal and its traffic interfaces considered by 'ConFlowGen'

2 ON TRAFFIC SCENARIO GENERATION WITH CONFLOWGEN

The tool 'ConFlowGen' aims to provide comprehensive, synthetic but yet realistic scenarios in a machine- readable data format for application in simulation studies or other data-driven applications. It's perspective focuses on container terminals including their interfaces to different modes of transport (see Figure 1). ConFlowGen allows users to quickly adjust their scenario inputs (e.g. vessel schedules, properties or distributions) and provides human-readable descriptions and analyses for the resulting scenario.

In order for ConFlowGen to generate scenarios, some input data are required. First, assumptions about vehicles as well as their properties and arrival information (e.g. schedules) need to be put in. This can be done for deep sea vessels, feeders, barges, and/or trains. The user can either provide comprehensive sailing lists in a tabular format or define the schedules by setting individual arrival frequencies and the number of inbound containers. As the only vehicle type, trucks are created according to the demand resulting from the other transport modes while approximating the truck arrival distribution at the same time. The number of outbound containers for each vehicle is determined by the number of inbound containers in combination with the assumed modal split. An example for such an origin-destination container flow on vehicle type level is shown in Figure 4. ConFlowGen also needs inputs about container properties, including expected distributions of lengths, weights, types, dwell times, and their destinations. Lastly, ConFlowGen expects some general scenario details. This includes the first and last day of the schedules to be considered and the vehicle type-dependant modal splits.

During the generation process, vehicle instances are generated according to the provided schedules. For each vehicle, the required amount of container instances is generated that it delivers to the container terminal on its inbound journey. Based on the origin-destination container flow distribution and the container dwell times, each container is assigned a later vehicle to leave the terminal again. In the beginning, ConFlowGen starts with an empty yard, and after the very last vehicle has departed, the yard is empty again.

After the generation process, ConFlowGen can export the resulting containers and vehicles including all their properties and transportation details in an instance-based, tabular format for further data processing in other software. In addition, ConFlowGen also provides comprehensive statistical information, analyses, and visualisations for the generated scenario. In detail, ConFlowGen provides two major types of output. In addition to the resulting data including corresponding visuals after the generation process, ConFlowGen also provides detailed previews for the user before the generation process. These assist the user to cross-check their input data and to estimate the impact of those inputs. This is further elaborated in Section 4.2.

3 METHOD

To vividly demonstrate the purpose, functionality, and features of the tool, in this paper ConFlowGen is applied and described along an exemplary use case. In this use case, a traffic scenario is generated and analysed in depth, which is based on real-life data of the Container Terminal Tollerort (CTT) in Hamburg, Germany. The example scenario uses publicly available information such as vessel arrival data and the published port modal split. Step-by-step, our assumptions and input data that are used to generate the traffic scenario are explained. Afterwards, the resulting synthetic scenario is analysed, discussed and visually validated together with our made assumptions.

In the first step, it is shown how ConFlowGen supports to calculate the numbers. Just by providing the assumed traffic distribution and vessel arrivals, the dimensions of the container volume from and to the hinterland are automatically determined. This functionality is called preview in ConFlowGen because it is just a rough calculation and not yet a scenario with actual vehicle and container instances. The second step covers the actual generation of the synthetic traffic scenario and the calculation of descriptive statistics. These results should be close to the initially used distribution parameters (e.g. container dwell time, truck arrival distribution, etc.). Such traffic scenario instances are then subject to analysis. The run analyses are based on container instances and consumable by, e.g. simulation models and/or digital twins.

Within this paper's exemplary use case, we demonstrate how ConFlowGen can provide valuable assistance when dealing with planning and layout problems, as well as other terminal-related questions.

Typical questions where ConFlowGen may be a helpful solution are, e.g. the following:

- Seaside: What is the expected seaside throughput? How large are the peaks created by delayed vessels?
- Hinterland: How many trucks are expected per day or hour to pass the truck gate of the terminal?
- Yard: How many ground slots are needed? What is the required stacking height?

Once we have arrived at a traffic scenario of such detail, the expectations of the container terminal yet to be planned are set. Surely, the amount of traffic must be somehow handled at each interface, i.e. long queues must be avoided as well as traffic jam inside the terminal. Likewise, all the containers must be accommodated in the laden and empty container yard so that sufficient capacity must be available. Based on the traffic scenario, each of the subsystems can be dimensioned accordingly. This is what ConFlowGen also supports by creating matching analyses.

Next, the planner needs to examine the system behaviour and to estimate the actual productivity of the terminal and its subsystems (e.g., seaside, berth, laden container yard, empty container yard, truck gate, and rail gate). As the interaction of the subsystems is complex, this is further analysed best within a simulation study based on traditional simulation models or more detailed digital twins. ConFlowGen supports the export of traffic scenarios to default tabular formats that are digestible by such software.

4 A SYNTHETIC DATA GENERATION USE CASE

In this chapter, ConFlowGen is exemplary applied by creating, visualising and discussing a synthetic traffic scenario based on the existing container terminal CTT in Hamburg, Germany.

4.1 Scenario Description

For our use case, we focus on the month of June 2022 as the observation window. To take into account unavoidable ramp-up and ramp-down processes in the resulting traffic flow data (see Section 4.5; Figure 7), vessel data was also accumulated for the two weeks before and after the observation window, which results in a total data time frame of eight weeks (mid of May to mid of July).

To replicate the modal splits for all possible transport mode relations (vehicle type dependant modal splits), ConFlowGen already includes multiple universally valid distributions as default values. To match the individual characteristics of the Port of Hamburg 's and CTT's overall

modal split (which is regu- larly published by the Port of Hamburg) we adapted minor parts of ConFlowGen's default values to approximate the scenario output.

For the seaside of the scenario, a publicly available sailing list, published and maintained by Hamburger Hafen Logistik AG (HHLA), was used to deduct the quayside traffic pattern [Hamburger Hafen und Logistik AG, 2023]. The original sailing list data contained 352 entries of arriving vessels of different types and sizes for the given time frame. We filtered the data and distinguished the vessels into two main categories, namely deep sea vessels and feeders, while (for reasons of brevity) excluding non-commercial vessels, tug boats, supply vessels, as well as barges from the data set. The resulting data set includes 236 port calls and is depicted in Figure 2. The vessel sizes cover a range of 124 twenty foot equivalent (TEU) units to 23,992 TEU with accumulations at around 1,000, 5,500, 14,000 and 20,000 TEU. The distinction between feeders and deep sea vessels is defined in the data set and was not conducted by the authors. It can be seen, that the resulting seaside traffic data over time consists of frequent port calls of the rather small feeders together with rarer but regular port calls of the larger deep sea vessels.

For arriving vessels, we assume that 30 %-60 % of the loaded containers of deep sea vessels are handled at the terminal, using a triangular distribution. For feeders, the handling ratio is set to 30 %-80 %. Those values are based on Park and Suh (2019). ConFlowGen distinguishes different container types via distributions. To keep the scenario simple, we stick to the default container type distribution [Kastner & Grasse, 2021].

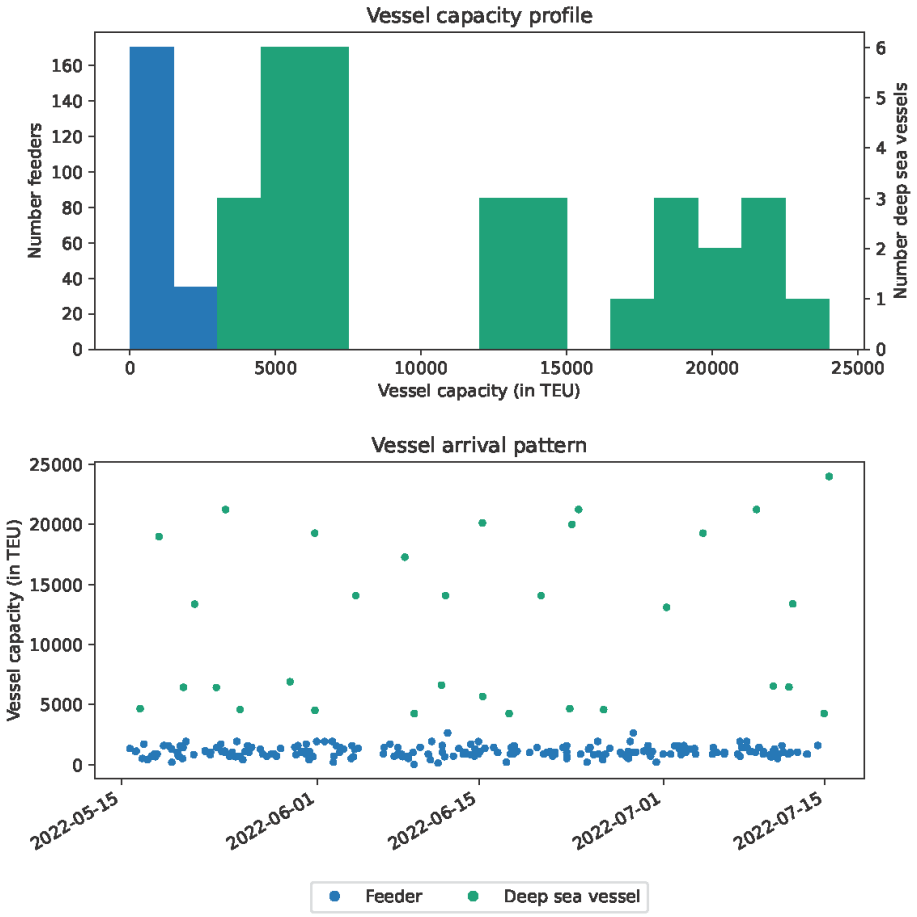

Figure 2: The vessel capacity profile and vessel arrival pattern

Regarding the amount of trains connecting the terminal, no comprehensive data was publicly available. To generate sufficient rail traffic (train visits) for the scenario, we therefore determined the necessary number of trains for each weekday to fulfil the scenarios overall transport requirements induced by the other modes of transport. We assume, that an average train can load up to 96 TEU and use ConFlowGen's default distribution for the train utilisation.

To keep the exemplary scenario brief and easy to understand we used some further simplifications. Barges and inland vessels are fully ignored in this scenario, which is acceptable since they are only re- sponsible for a rather small traffic volume share. Also, we do not account for deep sea to deep sea transshipment (interlining), since Hamburg is not a major interlining-transshipment hub but rather has a strong hinterland connectivity. For simplification, also feeder-to-feeder transshipment is ignored. Furthermore, we only account for 20' and 40' container sizes while ignoring other dimensions such as high cubes, 45' containers, open boxes, etc. 20' and 40' containers are considered in a 1/3 to 2/3 ratio [Statistisches Bundesamt, 2022].

4.2 Reviewing the Input Data

As previously mentioned, ConFlowGen can not only create synthetic data and its analyses after an elaborated generation process, it also provides the user with a fast and guiding feedback, called previews. Previews provide a first impression on what kind of data will be generated based on the set input distributions and schedules. At this stage, some internal simplifications are made to save calculation time. Among others, no container instances are generated and operational constraints are neglected.

The preview function is designed to answer typical rough-planning user questions like 'Will my modified schedule input still match my modal split between trucks and trains?'.

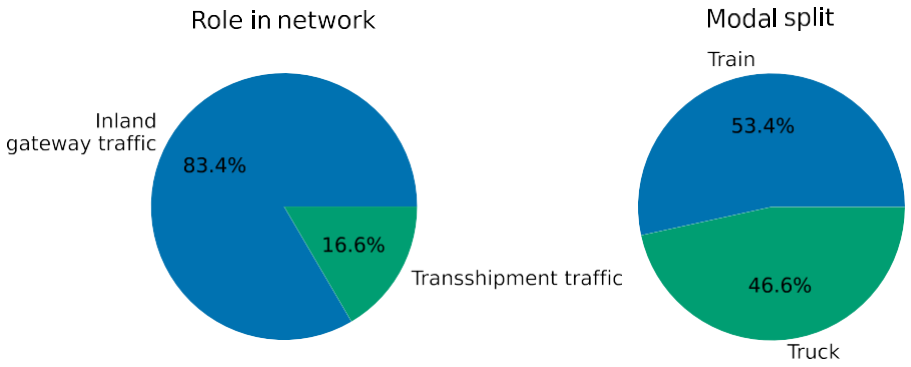

Figure 3: The role of the terminal in its network and the modal split in hinterland as estimated based on the distributions alone

In Figure 3, two typical previews derived from the use case are shown. The left pie-chart depicts the role in network via the estimated relation of inland gateway traffic and transshipment traffic. ConFlowGen determines those without generating each of the container or vehicle instances. It is just an estimation based on the distributions which contain seaside to seaside (transshipment) and seaside to landside (inland gateway) transport relations. If the scenario, e.g. aims for a 20 % transshipment, planning the inputs can be adapted instantly without running the generation. On the right side, the resulting modal split between the two modes train and truck is estimated. In our example use case, we aimed for a slight surplus on the train side, which is observable in the later analyses figures as well.

After having an appropriate input scenario set and performed a visual inspection of our previews for plausibility, we can start the actual generation. This will give us the container flow data needed together with comprehensive analyses and figures.

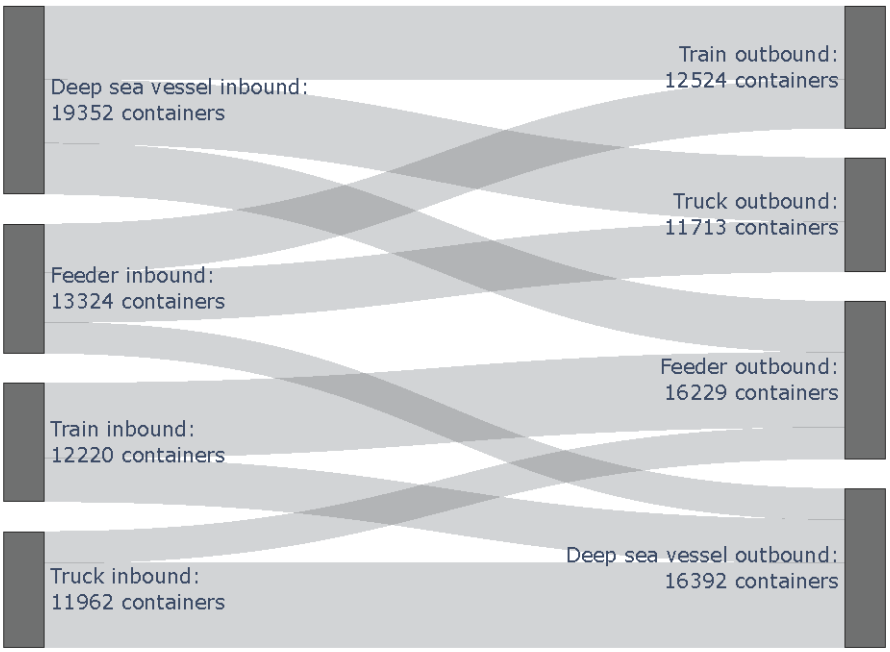

Figure 4: The container flow from its inbound vehicle type to its outbound vehicle type for June 2022 measured in containers

4.3 Summarising the Generated Container Flow

After execution of the generation process, we can now take a look into the data outputs and the corresponding analyses. Each container is delivered to the terminal by one vehicle on its inbound journey and is picked up again to leave the terminal by a second vehicle on its outbound journey. This relations are depicted in Figure 4 as a Sankey diagram. For the created scenario, there are around 19,000 containers delivered via deep sea vessels, which are then transported further on trains, trucks and feeders. On the output side, the terminal exports around 16,000 containers via deep sea vessels. Therefore, regarding the deep sea traffic, the terminal can be characterized with a slight import surplus. It can be seen, that there is no direct deep sea to deep sea transshipment in the scenario. The same can be seen for feeders as there is no connection between the feeders on the inbound side (shown left) and the outbound side (shown right). Moreover, the modelled terminal implies an overall strong rail connectivity, since more than 50 % of the hinterland's inbound and outbound traffic is transported via trains. Each of those characteristics match our given scenario inputs and previews.

For each type of container (i.e. standard, reefer, empty, and dangerous goods) and inbound-outbound relationship (i.e. each pairwise combination of deep sea vessel, feeder, train, and truck), one container dwell time distribution is assumed. Exemplary, the container dwell time distribution for standard containers from deep sea vessels to trucks are depicted in Figure 5. The figure shows *ConFlowGen*'s underlying input distribution for this exact transport relation (grey line), as well as a histogram representation of the dwell times of the generated container instances (blue beams). It can be seen, that most of the containers for this typical import relation stay within the terminal for around 40 hours until they are picked up by a truck and are transported to the

hinterland. A minimum processing time can also be identified in the figure, since even the fastest containers dwell for 10 to 20 hours. On the right side of the plot, it is visible that a small amount of containers need up to 210 hours until they are transported further. A distribution like this matches typical container terminals which charge a storage fee after a certain period of time.

In the case of deep sea vessels, feeders, and trains, containers are assigned their outbound vehicle according to the container dwell time and capacity availability of the vehicles. This ensures that all vehicles are working to their capacity. Trucks operate in a different way – they are created according to the truck arrival distribution in combination with the container dwell time distribution. In Figure 6, the distribution (scaled by the expected number of trucks per week for the time period) and the truck arrivals per hour at the truck gate for each calendar week (CW) are shown. The first line graph is plotted for the ISO CW 19 in 2022 which started on 9 May and lasted until 15 May. The last ISO CW 28 started on 11 July and lasted until 17 July. In other terms, the line graphs cover the whole range when vessels have been arriving at the terminal. The initially assumed truck arrival distribution is the default distribution as provided by ConFlowGen. In Germany, it is forbidden to transport goods on the road on Sundays. This even affects the Saturday afternoons when close to no-one starts or ends their journey at container terminals. The largest variation of the truck arrivals is seen on Thursdays and Fridays. Since at Sundays the truck gate is closed but the seaside operations continue, export containers must be delivered by truck before Sunday. Due to the low utilisation on Saturdays, this leads to peaks on Fridays. Similarly, if a container is discharged on a Sunday, this affects the truck gate throughput on the following days.

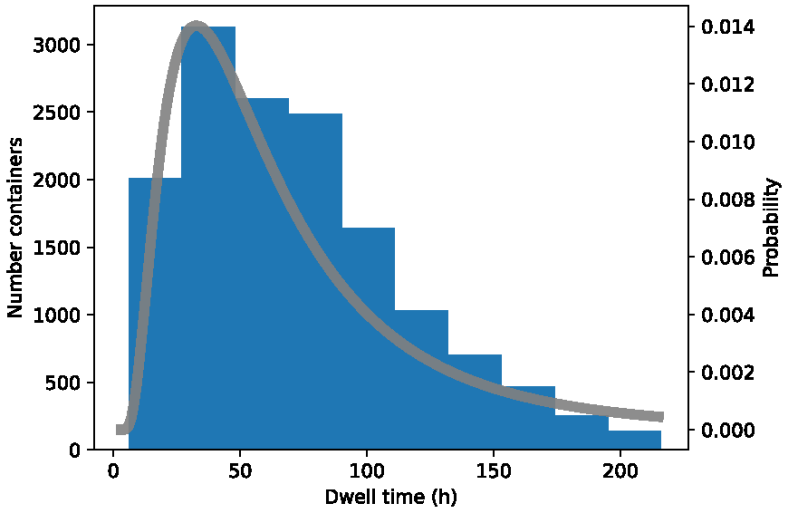

Figure 5: The container dwell time distribution for standard containers in June 2022 for the flow relation from deep sea vessel to truck

4.4 Filling and Emptying the Yard

When planning simulation studies, one might be tempted to start operations with a certain amount of containers inside the yard right from the beginning. This allows to approach busier operations faster. At the same time, however, each container might be moved by some equipment and thus the control systems must be able to access all relevant information regarding the arrival and future departure of a container. For each container, the information must be available and this is the reason why ConFlowGen generates this information independent from the later usage of the data inside the simulation. Even though the simulation might not start with an empty yard, from an information point of view there is a container that has arrived in the yard

first. Likewise, there is always a container that leaves the yard last. But does the yard fill level reach a steady state where for some period of time the inbound and outbound flows are evened out?

The yard fill level, the throughput at the truck gate and the vessel arrivals at the seaside are depicted in Figure 7. As ConFlowGen does not have any concept of container handling times, the vessels arriving at the quay are summarised by day (24 h window) and in terms of their TEU capacity. Especially deep sea vessels might take longer than a fraction of a day to be discharged and loaded before they depart again. In other terms, if one was to set up a simulation study and actually report the berthing times and actual seaside throughput, the graph would be much smoother. While the same is theoretically true for trucks at the truck gate, the impact of time-consuming activities is much lower, especially as they are summarised by 4h windows.

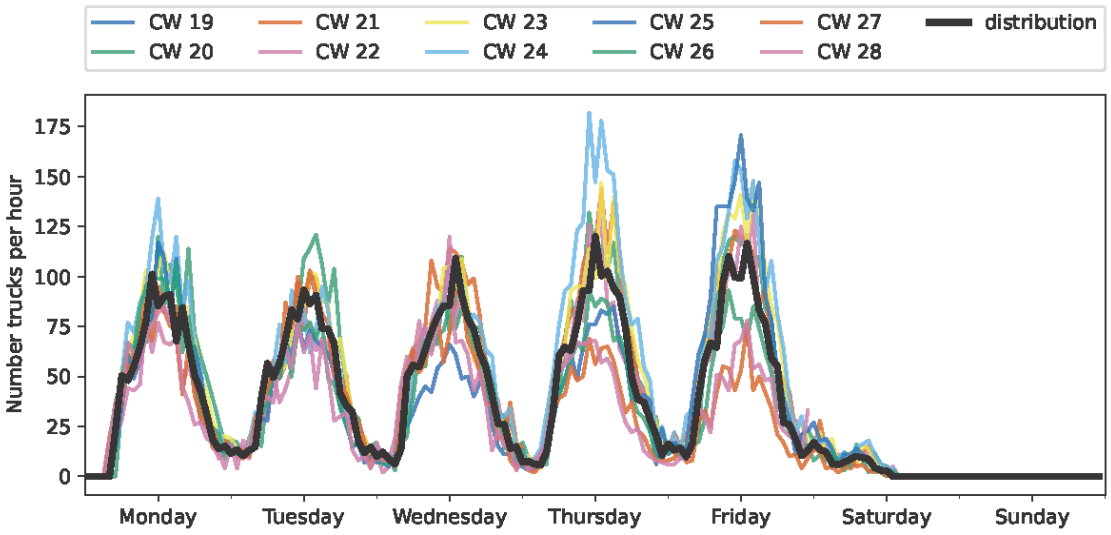

Figure 6: The initially set truck arrival distribution (in black) and the randomly drawn truck arrivals at the truck gate for each calendar week (CW)

The first containers are delivered to the terminal by truck even before May (see Figure 7). These activities are very unlikely and rare in number. First clearly visible activities start in the first week of May. During this time, the containers which will be placed on vessels on their outbound journey are delivered. Starting from 15 May, the truck gate throughput seems to be in a steady state until approximately 15 July. This is the same time period during which vessels arrive at the seaside. In the last week of July and in August, the last containers that are still in the yard are picked up by trucks – until the yard is empty again.

The used yard capacity in Figure 7 starts to grow slowly over May but has reached a steady state at 20,000-25,000 TEU even before the beginning of June. The peaks at the seaside directly impact the yard fill level. At the beginning of July, the yard fill level starts to drop again and it is far below 5,000 TEU even before August begins. This yard fill level seems reasonable when compared to other terminal figures such as the 'Container Terminal Altenwerder' with 39,000 TEU [Brinkmann, 2005, p. 312]. Moreover, the terminal capacity can be estimated based on the terminal area and the estimated TEU per hectare. When assuming that straddle carriers can stack 500 TEU per hectare [Brinkmann, 2005, p. 244] and the terminal area is 60 hectare [HHLA, 2022], then the total

capacity is approximately 30,000 TEU. Given the challenging shape of the terminal [HHLA, 2022], even a yard capacity lower than 30,000 TEU is reasonable.

4.5 A Closer Look at the Ramp Up and Ramp Down Period

In the previous section, the long period of a steady state in the yard is shown. During June 2022, the yard fill level fluctuates slightly and this reflects the change of yard utilisation in real-life data. The phase from May until the beginning of June is the ramp-up period. The yard fill level in Figure 7 starts at zero and quickly approaches 20,000 TEU. The phase from the end of June until August is the ramp-down period during which the yard fill level decreases back to zero. The ramp-up and ramp-down period are necessarily part of the data generation because logically one vehicle must be the first to deliver a container to the terminal and one vehicle must be a last to pick up the last container from the terminal. The ramp-up and ramp-down periods do not reflect the main phase of operation and these time periods might thus be excluded from performance evaluation. But how is the steady state of the system achieved? This is explored in the remainder of this subsection.

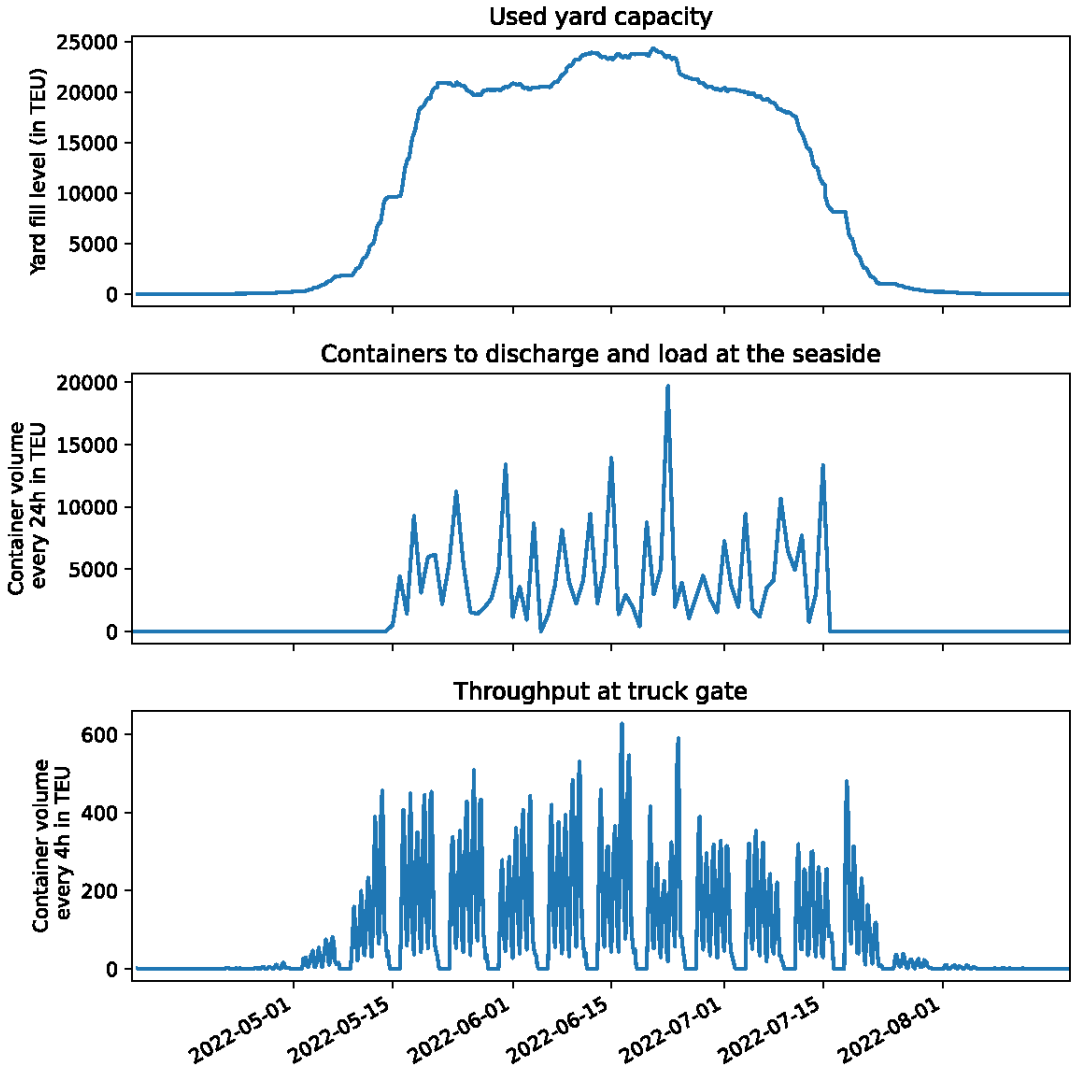

Figure 7: The relationship of yard fill level, vessel arrivals, and truck arrivals

In the previous Figure 7, the earlier truck arrivals have been depicted. Generally, trucks are the earliest means of transport that arrive at a container terminal. They start to fill the yard for specific other vehicle types, similar to the distribution indicated by the Sankey diagram in Figure 4. Thus, there are some containers to be loaded onto the first deep sea vessels and feeders to arrive. Starting from 15 May, deep sea vessels, feeders, and trains start to arrive. As visible in Figure 8, more containers are discharged from the first vehicles than there are containers being loaded onto them. Trains start at an outbound-to-inbound ratio of close to 0 %, i.e. they leave the terminal (nearly) empty. Feeders start with an outbound-to-inbound ratio of 80 %, i.e. much closer to the balanced 100 % ratio. Over the next days, the ratio increases until a steady state of the inbound-to-outbound ratio is reached. The steady state ratio can be deduced from Figure 4. If there are more outbound containers for a vehicle type than inbound containers, as it is the case for feeders, then the expected outbound-to-inbound ratio is expected to be larger than 100 %. This means that in this case more containers are loaded onto feeders than discharged. Such unpaired container flows exist in real life due to trade imbalances and complex empty container repositioning approaches. The trains never reach an outbound-to-inbound ratio of over 100 % because they are assumed to be block trains that arrive at the container terminal fully loaded and also depart again fully loaded. Feeders and deep sea vessels are capped at 120 % outbound-to-inbound ratio while also satisfying the TEU capacity constraint of each vehicle. The cap value is a flexible assumption that could be changed by a user at any time.

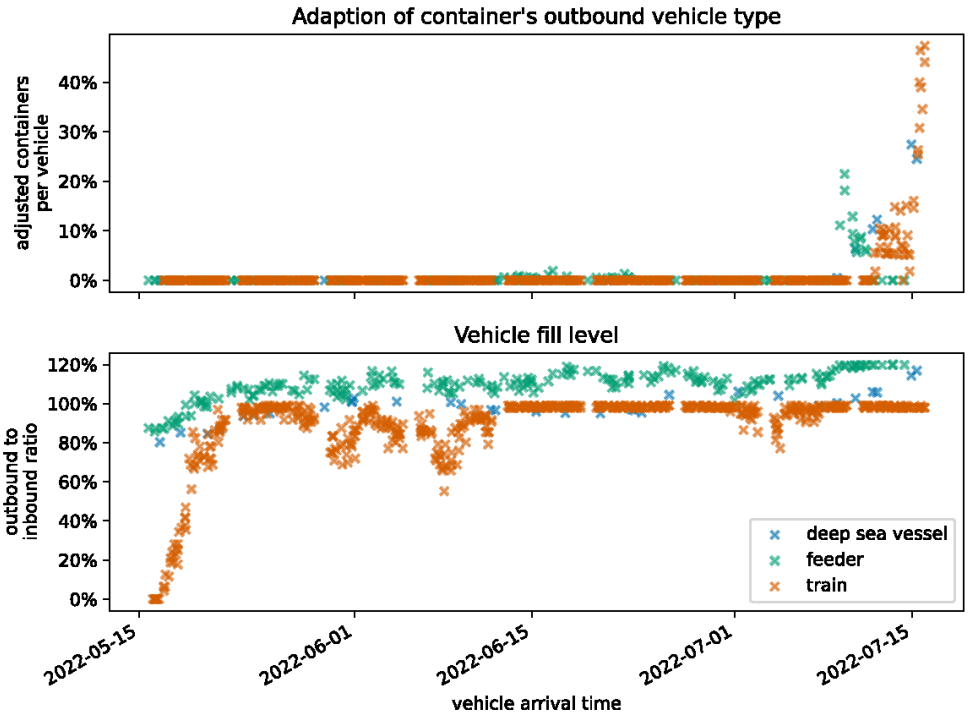

Figure 8: Outbound to inbound ratio per vehicle and the share of containers per vehicle that had to be assigned a new vehicle type

In the steady-state phase, there are a few disturbances depicted in Figure 7. Trains are sometimes not completely filled with containers. This is due to the assumed container dwell times in combination with the vessel arrival pattern. On 5 June, Pentecost took place in Germany that slowed down business activities all over the country and are thus also part of the vessel arrival patterns.

In the ramp-down phase starting in July, the outbound-to-inbound ratio slightly increases. Trains continue to be fully booked on their outbound journeys and feeders that used to already show a high outbound-to-inbound ratio now repeatedly reach the cap of 120 %. The deep sea vessels that are less in number but larger in impact on the yard now also show an outbound-to-inbound ratio of more than 100 %. The last deep sea vessel even approaches 120 %. Due to the non-existence of further vehicles after 15 June, all containers destined to leave the yard by a certain vehicle type are packed on a vehicle of the corresponding type. In some instances, this would lead to constraint violations (either the 120 % cap or the TEU capacity of the vehicle would be exceeded). In those instances, the vehicle type for the outbound journey of the container is adjusted and an alternative vehicle is looked up. In Figure 8, the share of containers that have undergone such adjustment is shown. Generally speaking, these adjustments can happen even in the steady state phase when minor supply chain hick-ups occur. The ramp-down phase of the terminal corresponds to a major change in the supply chain and thus a large amount of adjusted containers is reasonable. In the last week of July, the share of adjusted containers per vehicle (here: trains, feeders, and deep sea vessels) goes up to over 40 % for trains and 20 %-30 % for the last two deep sea vessels. Also for feeders, values beyond 10 % are recorded. This re-assignment of containers to new vehicle types might skew the overall inbound-to-outbound flow (compare Figure 4) because vehicles are chosen according to their availability. This is another argument why the last phase might show more artifacts of the synthetic generation. Thus, it is recommended to stop recording performance metrics before the ramp-down period starts and exclude it from further evaluation.

In summary, the steady state of the yard can be observed from two perspectives. First, the yard fill level shows a clear ramp-up and ramp-down period as well as a long-lasting steady state in between. Second, the ramp-up and ramp-down period are identifiable by vehicle properties. The ramp-up period is distinguishable from the steady state period by a lower outbound-to-inbound ratio per vehicle. This ratio later increases until it reaches a steady state. During the ramp-down period, more containers are re- assigned to outbound vehicle types according to the remaining transport capacities. The mechanisms that lead to this specific ramp-up and ramp-down behaviour are part of the general algorithm of ConFlowGen. Currently, it is up to the user to identify the steady state visually and decide which time period is representative enough for the simulation study or terminal planning task at hand.

5 CONCLUSIONS

In this paper, we introduce our synthetic data generation software and we show how to create valid, comprehensive container traffic scenarios with ConFlowGen for container terminals. The data is generated based on few assumptions and minimal information; it might further serve as an input for a simulation study time-efficiently. Even if just the traffic scenario itself is thoroughly examined (without running a simulation study), several insights can be generated.

When planning the terminal layout based on average values instead of concrete traffic scenarios, the outcome is supposed to be very similar. But especially when supply chain hick-ups or complex planning decisions are to be considered, it might be expedient and even easier to work with container instances in a detailed traffic scenario than with abstract expected values. When using concrete container traffic examples, aspects like the variation in yard fill level or the required throughput at the various terminal interfaces are already clearly visible. The variation of vessel arrivals based on example data are a more hands-on approach. ConFlowGen allows the users to estimate appropriate buffer capacities for the yard and the terminal interfaces based on likely scenarios.

With ConFlowGen, we have developed and introduced a convenient way to synthetically generate container flow data for detailed planning tasks and comprehensive scientific purposes with a sufficiently high quality. Nevertheless, the presented tool can also be understood and described as an intermediate or workaround solution to tackle a persistently predominant issue in research and applied science: real data are often scarce, confidential and/or hard to obtain, especially, e.g. from companies in highly competitive environments. Still, those kinds of data are essential to obtain innovative research results, develop new technologies and/or to generate new insights. Synthetic data generators like ConFlowGen cannot solve this fundamental issue but may alleviate it at least a little bit.

6 REFERENCES

Brinkmann, B. (2005): "Seehäfen: Planung und Entwurf", Springer Berlin Heidelberg.

Chu, C.-Y. & Huang, W.-C. (2005): "Determining Container Terminal Capacity on the Basis of an Adopted Yard Handling System", Transport Reviews, 25 (2), 181–199. DOI: 10.1080/0144164042000244608.

Hamburger Hafen und Logistik AG (2023): "HHLA Coast Report". Retrieved from **https://coast.hhla.de/segelliste**.

Hartmann, S. (2004): "Generating Scenarios for Simulation and Optimization of Container Terminal Logistics", OR Spectrum, 26 (2), 171–192. DOI: 10.1007/s00291-003-0150-6.

HHLA (2022): "Technische Daten Tollerort (CTT)". Retrieved from **https://hhla.de/unternehmen/tochterunternehmen/container-terminal-tollerort-ctt/technische-daten**.

Kastner, M. & Grasse, O. (2021): "ConFlowGen Documentation". Retrieved from **https://conflowgen.readthedocs.io/en/latest/index.html**.

Kastner, M., Grasse, O. & Jahn, C. (2022): "Container Flow Generation for Maritime Container Terminals". In: "Dynamics in logistics", Proceedings of the 8th International Conference LDIC 2022", Bremen, Germany (pp. 133-143), Bremen, Germany: Springer Cham. DOI: 10.1007/978-3-031-05359-7 _11.

Kastner, M., Lange, A.-K. & Jahn, C. (2020): "Expansion Planning at Container Terminals". In: M. Freitag, H.-D. Haasis, H. Kotzab & J. Pannek (Eds.): "International Conference on Dynamics in Logistics" (LDIC 2020) (pp. 114-123), Springer International Publishing. DOI: 10.1007/978-3-030-44783-0_11.

Park, N.K. & Suh, S.C. (2019): "Tendency Toward Mega Containerships and the Constraints of Container Terminals", Journal of Marine Science and Engineering, 7 (5). Retrieved from **https://www.mdpi.com/2077-1312/7/5/131 DOI: 10.3390/jmse7050131**.

Port Planning and Construction Committee (2001): "IAPH Guidelines for Port Planning and Design", International Association of Ports and Harbors (IAPH).

Statistisches Bundesamt (2022): "Statistisches Bundesamt". Retrieved from **https://www.destatis.de/DE/Themen/Branchen-Unternehmen/Transport-Verkehr/Gueterverkehr/Publikationen/Downloads-Schifffahrt/seeschifffahrt-monat-2080500211084.pdf**.

UNCTAD (2020): "UNCTAD 2020", Geneva. Retrieved from **https://unctad.org/system/files/official-document/rmt2020en.pdf**.

Wiese, J., Suhl, L. & Kliewer, N. (2011): "Planning Container Terminal Layouts Considering Equipment Types and Storage Block Design". In: J.W. Böse (Ed.): "Handbook of Terminal Planning" (pp. 219-245), New York, NY: Springer New York, DOI: 10.1007/978-1-4419-8408-1_12.

SUMMARY

More than 80 % of world trade is delivered via sea, making the maritime supply chain a very important backbone for the economy [UNCTAD, 2020]. Containerised trade regularly outperforms other types of transport in terms of growth, coinciding with consistent increases of average container vessel sizes [UNCTAD, 2020]. Container terminal operations are heavily affected by this development, since less but larger port calls create unwanted peaks and stress on the terminals and the hinterland. Not all container terminals are affected equally by the described situation. Economic cycles and events such as the global COVID-19 pandemic or the Russian war in Ukraine change the global supply chains, trade characteristics and transport demands between ports in the world.

In 2004, Hartmann proposed an approach to create scenarios for simulation and optimisation in the sense of container terminal planning and logistics [Hartmann, 2004]. Due to the significant changes in maritime trade over the years, a new approach for generating synthetic container flow data became practical. In 2021, we introduced a rethought and reworked approach on this topic. The proposed tool, named ConFlowGen, aims to assist planners, scientists, and other maritime experts with providing comprehensive container flow scenarios based on minimal inputs and assumptions of the user. In this paper, we introduce ConFlowGen's general principle of operation in an exemplary use case in the context of container terminal planning.

RESUME

Plus de 80 % du commerce mondial est acheminé par voie maritime, ce qui fait de la chaîne d'approvisionnement maritime une épine dorsale très importante pour l'économie [UNCTAD, 2020]. Le commerce conteneurisé dépasse régulièrement les autres types de transport en termes de croissance, ce qui coïncide avec l'augmentation constante de la taille moyenne des navires porte-conteneurs [UNCTAD, 2020]. Les opérations des terminaux à conteneurs sont fortement affectées par cette évolution, car des escales moins nombreuses mais plus importantes créent des pics et des tensions indésirables sur les terminaux et l'arrière-pays. Tous les terminaux à conteneurs ne sont pas affectés de la même manière par la situation décrite. Les cycles économiques et les événements tels que la pandémie mondiale de COVID-19 ou la guerre russe en Ukraine modifient les chaînes d'approvisionnement mondiales, les caractéristiques commerciales et les demandes de transport entre les ports du monde entier.

En 2004, Hartmann a proposé une approche pour créer des scénarios de simulation et d'optimisation dans le cadre de la planification et de la logistique des terminaux à conteneurs [Hartmann, 2004]. En raison des changements importants survenus dans le commerce maritime au fil des ans, une nouvelle approche pour générer des données synthétiques sur les flux de conteneurs est devenue pratique. En 2021, nous avons introduit une approche repensée et retravaillée sur ce sujet. L'outil proposé, appelé ConFlowGen, vise à aider les planificateurs, les scientifiques et les autres experts maritimes à fournir des scénarios complets de flux de conteneurs sur la base d'un minimum de données et d'hypothèses de l'utilisateur. Dans cet article, nous présentons le principe général de fonctionnement de ConFlowGen dans un cas d'utilisation exemplaire dans le contexte de la planification des terminaux à conteneurs.

ZUSAMMENFASSUNG

Mehr als 80 % des Welthandels werden auf dem Seeweg abgewickelt, was die maritime Lieferkette zu einem sehr wichtigen Rückgrat der Wirtschaft macht [UNCTAD, 2020]. Der Handel mit Containern wächst regelmäßig schneller als andere Verkehrsarten, was mit einem stetigen Anstieg der durchschnittlichen Containerschiffsgrößen einhergeht [UNCTAD, 2020]. Der Betrieb von Containerterminals ist von dieser Entwicklung stark betroffen, da weniger, aber größere Hafenanläufe zu unerwünschten Spitzen und Belastungen für die Terminals und das Hinterland führen. Nicht alle Containerterminals sind von der beschriebenen Situation gleichermaßen betroffen. Wirtschaftszyklen und Ereignisse wie die weltweite COVID-19-Pandemie oder der russische Krieg in der Ukraine verändern die globalen Lieferketten, die Handelsmerkmale und die Transportnachfrage zwischen den Häfen der Welt.

Im Jahr 2004 schlug Hartmann einen Ansatz zur Erstellung von Szenarien für die Simulation und Optimierung im Sinne der Planung und Logistik von Containerterminals vor [Hartmann, 2004]. Aufgrund der erheblichen Veränderungen im Seehandel im Laufe der Jahre wurde ein neuer Ansatz zur Erzeugung synthetischer Containerflussdaten sinnvoll. Im Jahr 2021 haben wir einen neu durchdachten und überarbeiteten Ansatz zu diesem Thema vorgestellt. Das vorgeschlagene Tool mit dem Namen ConFlowGen soll Planern, Wissenschaftlern und anderen maritimen Experten dabei helfen, umfassende Containerflussszenarien zu erstellen, die auf minimalen Eingaben und Annahmen des Benutzers basieren. In diesem Beitrag stellen wir das allgemeine Funktionsprinzip von ConFlowGen anhand eines beispielhaften Anwendungsfalls im Kontext der Planung von Containerterminals vor.

RESUMEN

Más del 80 % del comercio mundial se realiza por vía marítima, lo que convierte a la cadena de suministro marítima en una columna vertebral muy importante para la economía [UNCTAD, 2020]. El comercio en contenedores supera regularmente a otros tipos de transporte en términos de crecimiento, coincidiendo con aumentos constantes del tamaño medio de los buques portacontenedores [UNCTAD, 2020]. Las operaciones de las terminales de contenedores se ven muy afectadas por esta evolución, ya que un menor número de escalas portuarias, pero de mayor tamaño, crea picos no deseados y tensiones en las terminales y en el interior. No todas las terminales de contenedores se ven afectadas por igual por la situación descrita. Los ciclos económicos y acontecimientos como la pandemia mundial de COVID-19 o la guerra rusa en Ucrania modifican las cadenas mundiales de suministro, las características del comercio y las demandas de transporte entre los puertos del mundo.

En 2004, Hartmann propuso un enfoque para crear escenarios de simulación y optimización en el sentido de la planificación y logística de terminales de contenedores [Hartmann, 2004]. Debido a los importantes cambios que se han producido en el comercio marítimo a lo largo de los años, se hizo práctico un nuevo enfoque para generar datos sintéticos sobre el flujo de contenedores. En 2021, presentamos un enfoque replanteado y reelaborado sobre este tema. La herramienta propuesta, denominada ConFlowGen, tiene como objetivo ayudar a planificadores, científicos y otros expertos marítimos a proporcionar escenarios completos de flujo de contenedores basados en entradas y suposiciones mínimas del usuario. En este artículo, presentamos el principio general de funcionamiento de ConFlowGen en un caso de uso ejemplar en el contexto de la planificación de terminales de contenedores.

7 QUANTIFYING THE RISKS OF CLIMATE CHANGE ON INLAND WATERWAY TRANSPORT IN THE NETHERLANDS

JURJEN DE JONG

During the research: Researcher/advisor river dynamics and inland shipping at Deltares,
P.O. Box 177
2600 MH Delft
The Netherlands

Jurjendejong@gmail.com

Keywords: Climate change, inland waterway transport, infrastructure, the Netherlands
Mots-clés: Changement climatique, transport fluvial, infrastructure, les Pays-Bas

1 INTRODUCTION

Inland waterway transport (IWT) forms an important contribution to the transport of cargo in the Netherlands. Of the total freight transport, approximately 34 % is transported over water. IWT in the Netherlands uses a combination of shipping canals and rivers that have been normalised and canalised for improved inland navigation.

The Dutch trajectory of the river Rhine is a free-flowing river, and forms a major shipping route from the Port of Rotterdam to Germany with a fairway width of at least 150 m. The river is normalised by the construction of groynes and the removal of sharp bends. On a daily basis an average of 400,000 tonnes is transported over this route. The water levels are still susceptible to discharge variations and may limit IWT due to insufficient water depth (low flow) or insufficient clearance height (high flow).

The Dutch trajectory of the river Meuse is strongly canalised with the construction of lateral canals and weirs, and locks to pass these weirs. This shipping route is used primarily for national IWT, but also offers a connection to the Belgium network. All year, the water levels are controlled by the weirs, allowing sufficient water depth in the fairway. However, during low flow periods, the discharge in the Meuse is no longer sufficient to freely operate the locks, resulting in additional operational measures.

It may be clear that the discharge on the Rhine and Meuse is of importance for a reliable inland fairway network. As a result of climate change the discharge regimes of both rivers are expected to change. Thus, climate change may form a risk on the future reliability of inland navigation.

To gain insight into the current and future state of the system, the programme 'Climate Resilient Infrastructure Networks' was set up by the Dutch government within the national programme on spatial adaptation. One of the focus fields is the Inland Fairway Infrastructure (only those managed by the national government). The goal of the programme is to determine vulnerabilities, discuss with stakeholders and to set up a future agenda. In a series of stress tests, the effects of amongst others low flow and high flow are evaluated.

This paper will discuss three of those stress tests by making use of future climate change scenarios:

- The effects of low flow on a free-flowing river (on the Rhine)
- The effects of low flow on the operation of locks (on the Meuse)
- The effects of high flow on the clearance height at bridges

In all stress tests we quantified the effects for the inland waterway transport sector. Novel methods are set up using computational and analytical models. Each section can be read individually and is based on research from multiple reports.

All stress tests make use of future climate change scenarios for the years 2050 and 2085. Based on the global IPCC reports, the Royal Netherlands Meteorological Institute (KNMI) made a translation of climate change projections for the Netherlands. These KNMI '14 scenarios (Figure 1) are used to derive future river discharge series. Based on these scenarios, in other projects of Deltares a permutation of a 100-years discharge timeseries is made. Based on these discharge scenarios characteristic statistical years are developed for this paper that schematise a drought year with a return period of 1, 2, 10 and 100 years. This action is performed for scenarios G_L and W_H and for both the year 2050 and 2085 [De Jong, 2019 ; De Jong 2020a].

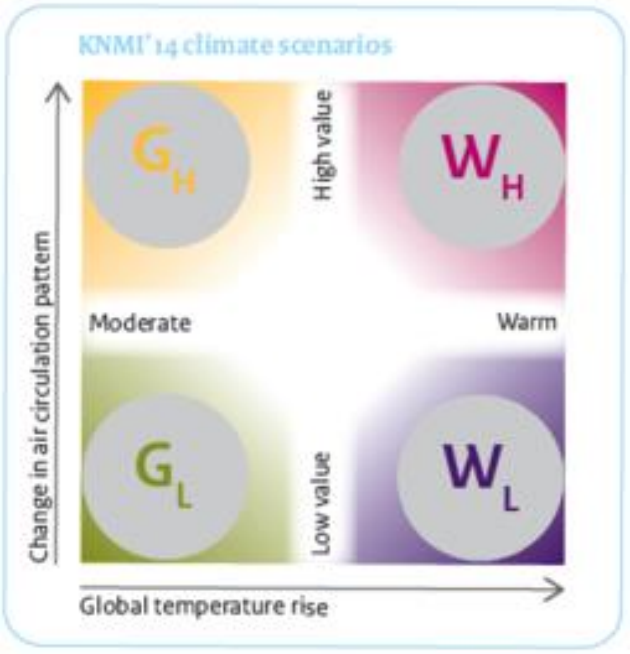

Figure 1: Climate scenarios by the KNMI (KNMI, 2015).

2 STRESS TEST ON THE EFFECTS OF LOW FLOW ON THE RHINE

2.1 Introduction

The draught of vessels on the river Rhine ranges between 1 and 4 m, with a median of around 2.5 m. During low flow conditions, the water depth is insufficient for all vessels to sail with their preferred draught and as a result the cargo (or load factor) need to be reduced to decrease the ship's draught. The remaining cargo is transported with additional ships or with other modalities, resulting

in higher transport costs. When this is no longer possible, the cargo is no longer transported resulting in larger economic consequences. In this study this increase in transport costs due to drought is quantified [De Jong & Van der Mark, 2021 ; De Jong, 2020b].

2.2 Method

To quantify the effects of low flow on the shipping sector in the current and future climate, a combination of models was set up.

2.2.1 Step 1: Modelling the Water Depth in the Fairway of Free-Flowing Rivers

Computing the water depth in the free-flowing rivers requires knowledge on the state of the river and the water discharge. The state of the river is continuously changing. Human interventions such as the construction of river engineering measures to improve flood safety and ecological quality of the river are executed every year. Most famous are the measures in the programme 'Room for the River' (in Dutch: 'Ruimte voor de Rivier'), which also include measures within the main channel of the river that influence the flow conditions during low flow. The Dutch government actively invests in the modelling of the accurate state of the river in different hydraulic models. This paper uses the one-dimensional (1D) SOBEK model which is also calibrated on low flow conditions. Models of the Rhine, Meuse and Rhine-Meuse-delta are merged into a combined model shown in Figure 2. Boundary conditions include the river discharge of the Rhine and Meuse and an average tidal boundary at the North Sea. As low flow conditions often coincide with drought, a major part of the river discharge is distributed to canals to assure amongst others the water quality in these canals. An estimate for each of those extractions is included in the model.

Figure 2: River branches in the combined 1D SOBEK model of the Maas/Meuse, Rijn/Rhine and Rijn-Maasmonding/Rhine-Meuse-delta. Several other locations that are mentioned later in this paper are also included.

For modelling future scenarios, it is required to include the ongoing trend in bed erosion and sedimentation in the model. These trends influence the discharge distribution over the Rhine branches and influence the water depth, especially around non-erodible bed layers in both the main channel and at locks. Measurements have shown that over the last 20 years local trends are averaging between –1.8 cm/year to +1.8 cm/year [Ylla Arbós, 2019]. Based on these trends, scenarios are developed for the expected bed level in 2050, including the change in trend that can be observed or is to be expected [Sloff, 2019]. For the Waal Branch (the main branch of the Rhine River) the trend is shown in Figure 3. The estimated future trend is imposed on the main channel of each cross-sectional profile as demonstrated in Figure 4.

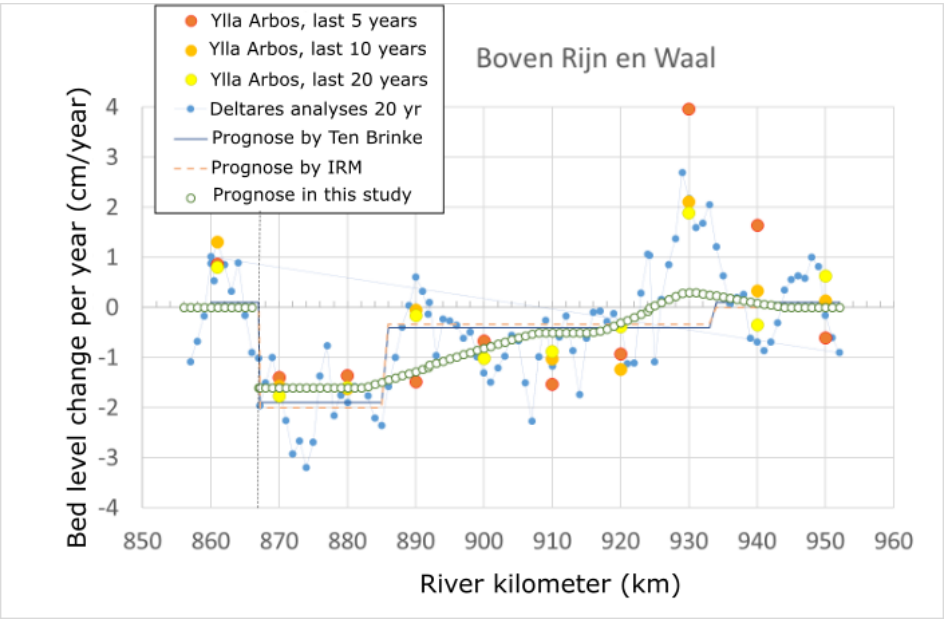

Figure 3: Bed level change along the river Rhine from measurements as analysed by Ylla Arbós (2019) and the expected future bed level change applied in this paper (green dots)

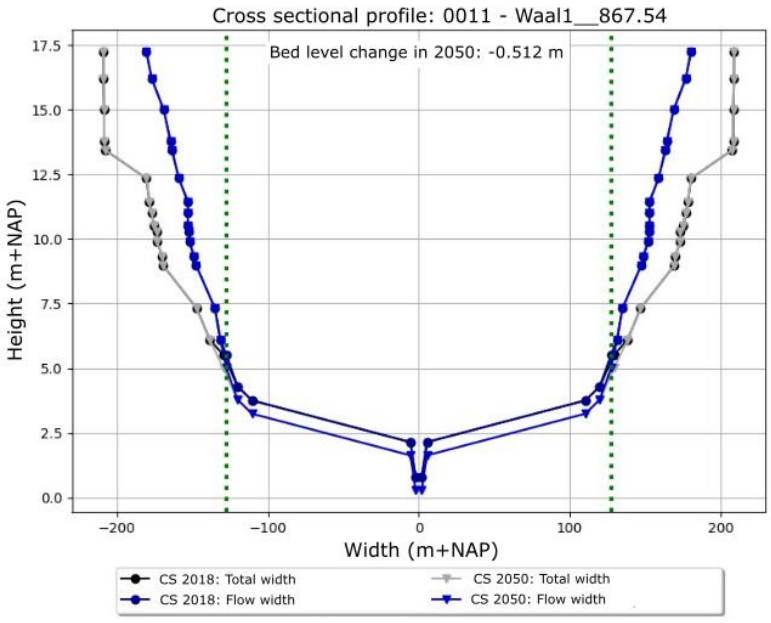

Figure 4: Example of a cross section on the Rhine where for the situation of 2050 the main channel (between the green lines) is corrected with a bed level trend of –0.512 m

The cross section as shown in Figure 4, also demonstrates that the main channel in the 1-D model is a strong simplification of reality. The schematisation is created by analysing the bed level over a stretch of 500 m, computing the bed level volume and translating this into the cross-sectional profile. In this process any information on river bedforms and shallow inner river bends is lost. However, this information is critical for an accurate water depth in the fairway. The water depth is therefore computed by imposing both the measured bed level and the computed water levels on a two-dimensional (2-D) grid and analysing this grid to find the best available fairway. A grid is constructed following the main channel with approximate cell width of 10 m and cell length of 300 m. To construct a bed level grid, in each grid cell the 95 % percentile highest value of all measurements (resolution of 1x1 m) is used as the normative bed level (

Figure 5). Using this process, the anomalies in the samples are filtered out while the effect of bedforms and shallows remains. The water level results of the SOBEK model are linearly interpolated to this grid. Subtraction per cell of water and bed level results in a 2-D grid of the water depth.

The water depth grid is analysed for the deepest available fairway. The minimum required width of each fairway stretch is defined by governmental regulations [Koedijk, 2020]. By interpolating the grid for a given channel width, the available water depth is found. However, during low flow conditions, the channel width may be reduced to allow for saver navigation and larger water depth. This is most apparent on the river IJssel, where the smallest sections are only 40 m. To take this into account in the grid, the interpolation is extended with a module where the required width can be slightly relieved when the minimum required depth (2.5 or 2.8 m) can no longer be obtained. A demonstration of this process is given in

Figure 6.

The resulting water depth of this step forms the building block for the shipping analyses.

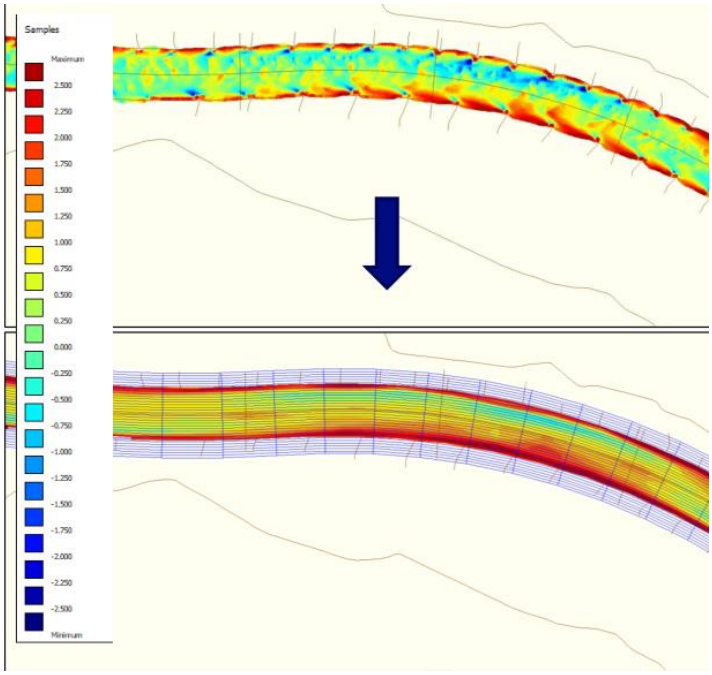

Figure 5: Process of transposing the high-resolution samples onto the bed level grid for a stretch of 3 km on the river Waal

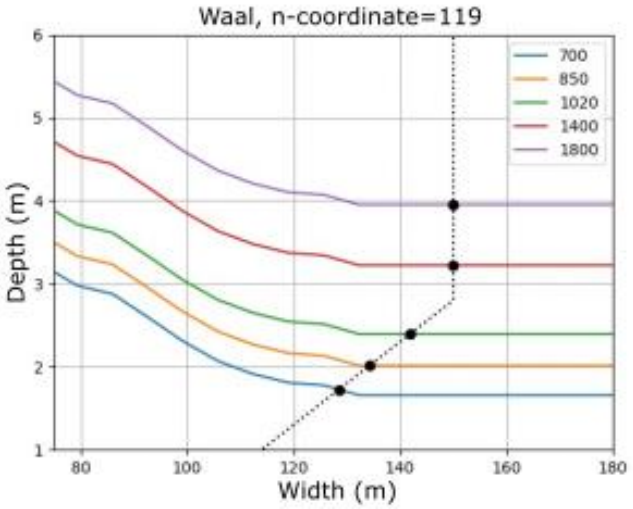

Figure 6: Example of the water depth as a function of the channel width for different discharges (coloured lines) for an arbitrary cross section on the Waal River. The dashed line indicates the minimum required width-depth combination. The crossings of the lines (black dots) give the resulting depth and width of the fairway channel.

2.2.2 Step 2: Modelling the Effect of Low Water Depth on the Shipping Sector

The effect of limited water depth on the shipping sector is computed by the numerical model BIVAS (Inland shipping analysis system, in Dutch BInnenVaart Analyse Systeem). This model is maintained by the Dutch government and contains a schematisation of all fairways in the Netherlands as well as important reaches in neighbouring countries (

Figure 7). The network is schematised with arcs between all ports and bifurcations. To each arc, the shallowest cross-section from the water depth grid is attributed, as well as flow velocities coming directly from the SOBEK model. This coupling is shown in Figure 8.

Another core component of the BIVAS model is a dataset of all annual trips over the network. The registration service IVS is used to develop this dataset. Each of the over 400,000 individual trips has unique information on amongst others the origin, destination, ship draught, cargo and the ship type. The registrations of the year 2014 are used as the reference situation with good sailing conditions during the entire year. We make use of this reference situation, as well as a future situation with economic growth.

During a run, the BIVAS model will find the cheapest way to transport the cargo over the network. The model (including corrections in the post-processing) will find the most efficient route and if necessary reduce the draught of the vessel. When the draught needs to be reduced, the reduction in cargo is computed using the metric TPCMI (Tons per centimetre immersion) of that specific vessel. It is assumed that the total transported cargo is to be kept constant, resulting in an increase in the number of trips. For example, if the cargo of a trip is reduced by 20 %, it is assumed to increase the trips by 25 %. Accordingly, all metrics of this trip are corrected by a factor 1.25. This is shown in the example in

Figure 9.

The most important metric is the variable sailing costs, consisting of costs for fuel, staff, insurance, interest, depreciation and maintenance. Each ship type has unique parameterisation to compute these costs from research by Panteia (2018).

Additionally, a correction is performed for the situation where reduction of cargo is more than 80 %.[1] In this case it is assumed to be no longer profitable for inland waterway transport. It is assumed that depending on the type of cargo, transportation will be either delayed or carried using a different modality. To simplify this economic analysis, it is assumed that the costs remain at the level costs of 80 % cargo reduction (an increase of 400 % with respect to the sailing costs without limitations in draught). In the figures this is referenced to as the costs for not-transported cargo.

[1] All post-processing scripts are available on **https://github.com/jurjendejong/pyBIVAS**.

Figure 7: Fairways in the BIVAS model for the year 2030. The network extends with European waterways outside this figure.

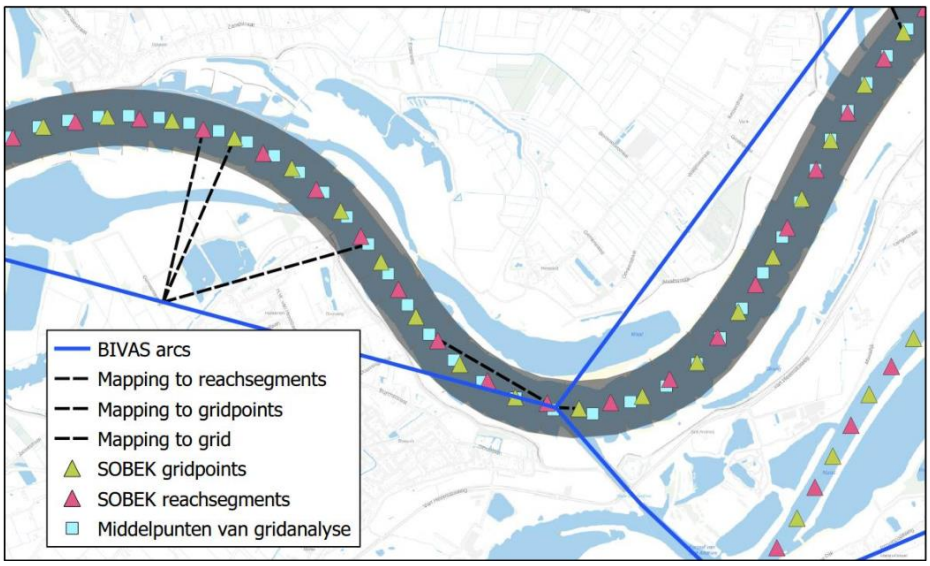

Figure 8: Example of a close-up of the arcs in the BIVAS model, and the coupling that is developed to the water depth grid and the SOBEK model.

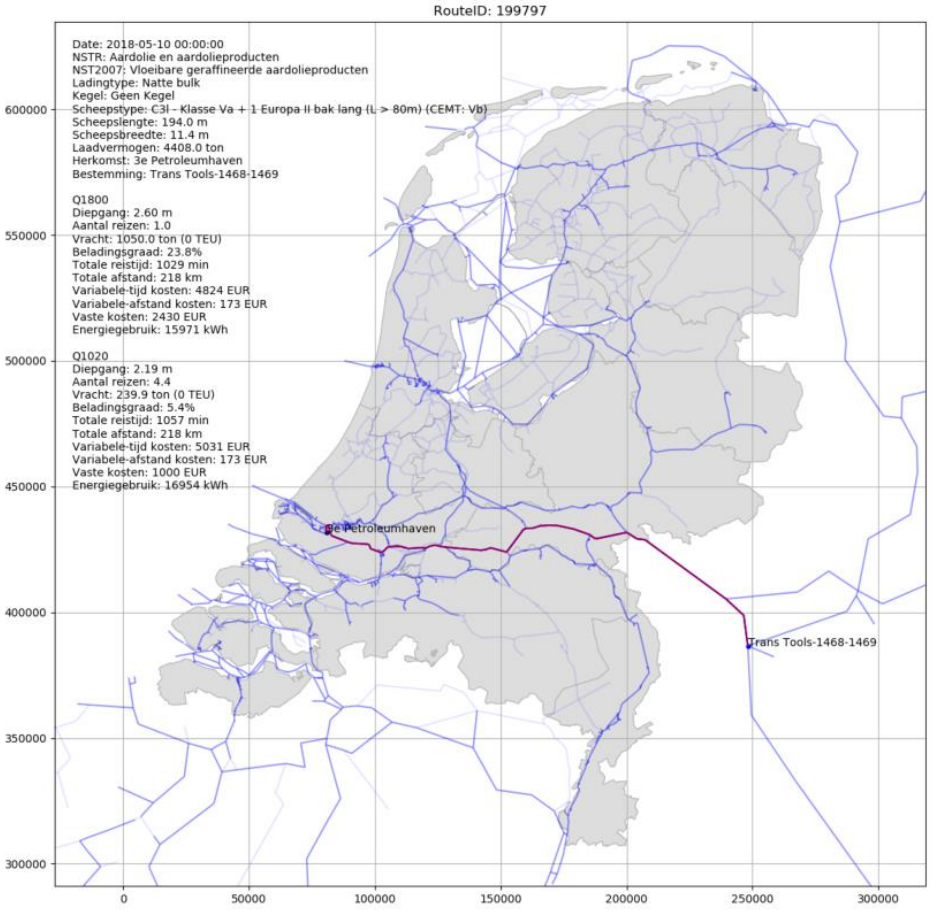

Figure 9: Example of a single trip as computed by BIVAS. The top block shows details on this trip from the IVS database, the second block and third block show trip details when the discharge on the Rhine is respectively 1,800 and 1,020 m^3/s. The different components are written in the figure in Dutch, but they give an indication of the extensiveness of the IVS database and the result of the BIVAS simulations.

2.3 Results

Results look both at the state of the fairway under climate change, as well as the consequences on the IWT. A selection of the results is given in the figures below.

Figure 10 shows that at a very low discharge of 700 m^3/s, the transport costs of the IWT sector increase by € 3 million per day with respect to the average of 6.3 million on a day without draught limitations.

Figure 11 shows that in a dry year (a long period of low discharge) with a return period of 10 years (T10), the total transport costs can increase with € 126 million. In a scenario with high climate change (KNMI scenario W_H), the costs in a T10 dry year increase to 263 million euro. Averaged over a longer period these costs are lower: € 48 million per day in the current climate, and 104

million with high climate change. Please note that the costs calculated are pure transportation costs; additional costs and cascading damage are not accounted for.

Using the results, it is discussed to what extent measures can be achieved to increase the state of the fairway. An increase in water depth in the order of 10 cm can be achieved with river engineering measures. For example, by construction of longitudinal training walls, as recently realised as a pilot on the river Waal. However, these measures cannot fully counteract the loss in water depth as a result of climate change.

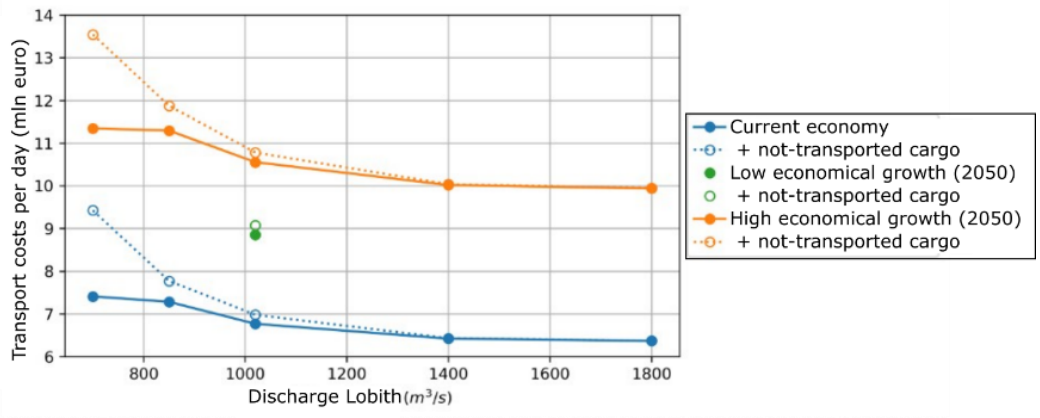

Figure 10: Total transport costs of the IWT in relation to the discharge on the Rhine at Lobith (at the Dutch German border). An assumption is done for the costs for the cargo that cannot be transported over water.

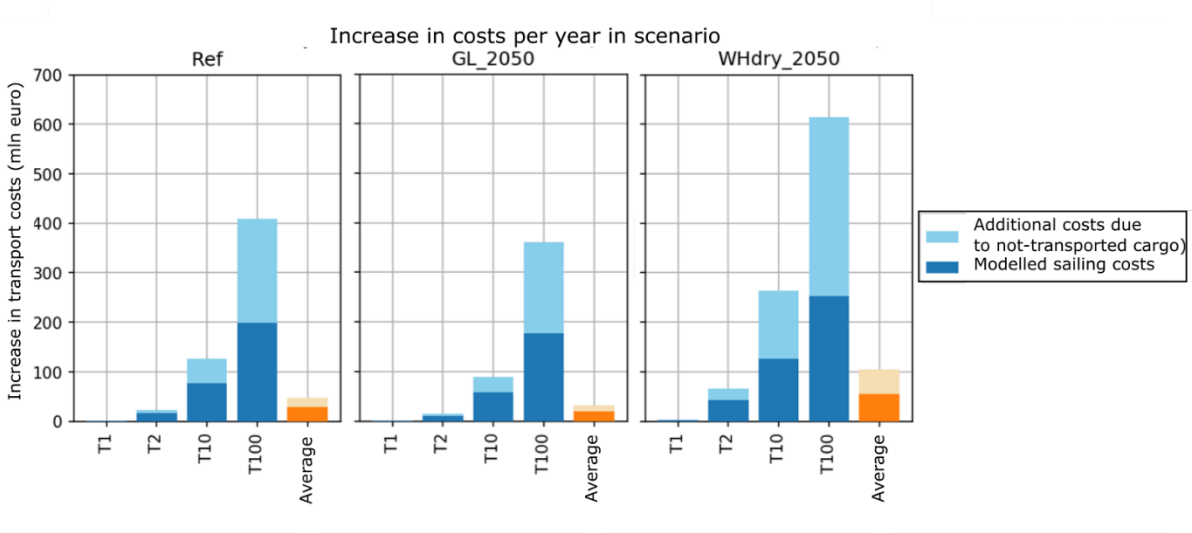

Figure 11: Increase in transport costs in low discharge years with a return period of 1, 2, 10 and 100 years, and the yearly average over a long time. For the reference scenario (left) and a scenario with moderate climate change (centre) and high climate change (right). These costs in a year without drought problems are approximately € 2 billion. An assumption is done for the costs for the cargo that cannot be transported over water.

3 STRESS TEST ON THE EFFECTS OF LOW FLOW AT LOCKS ON THE MEUSE

3.1 Introduction

The river Meuse is strongly canalised by the construction of weirs in both the Netherlands and Belgium. In the most upstream reach of the Netherlands, the Julianakanaal is constructed as a parallel canal to the Meuse (this reach of the Meuse is called the Grensmaas, a Nature 2000 area). The large head of the locks in this canal (up to 11.85 m) results in a significant water demand for lock operation. From discharge measurements it is shown that on average 17 m^3/s is required to operate the canal. However, during low flow conditions, the total discharge of the Meuse can fall below 25 m^3/s, which requires sparingly operation of the lock to save sufficient water for the Nature 2000 area and other users of the Meuse water.

The water demand of the levelling process can be reduced with a number of operational measures:

- Reducing the number of levellings by requiring a higher occupancy rate of the lock chamber (gentle or strict regime)
- Using pumps to return the water to the upstream canal
- Saving water in the levelling process by using a water basin or by siphoning between lock chambers

Each measure results in an increase in the operational costs, either by increasing the energy demand of the locks (when using pumps) or due to the increase in passage time of the vessels due to the longer waiting or levelling times (all other measures). To verify the reduction in water demand, Figure 12 shows the statistical relation between the discharge on the Maas and the discharge towards the locks. During low flow on the Maas, the water demand by the lock reduces from 17 m^3/s to below 5 m^3/s. However, a strategy is required on when to use which one of these measures such that it results in the lowest total costs. In this stress test [De Jong & Boschetti, 2020] different strategies are developed for each of the lock complexes. This also shows the annual damage as a result of drought, and the possible mitigation when installing additional infrastructure.

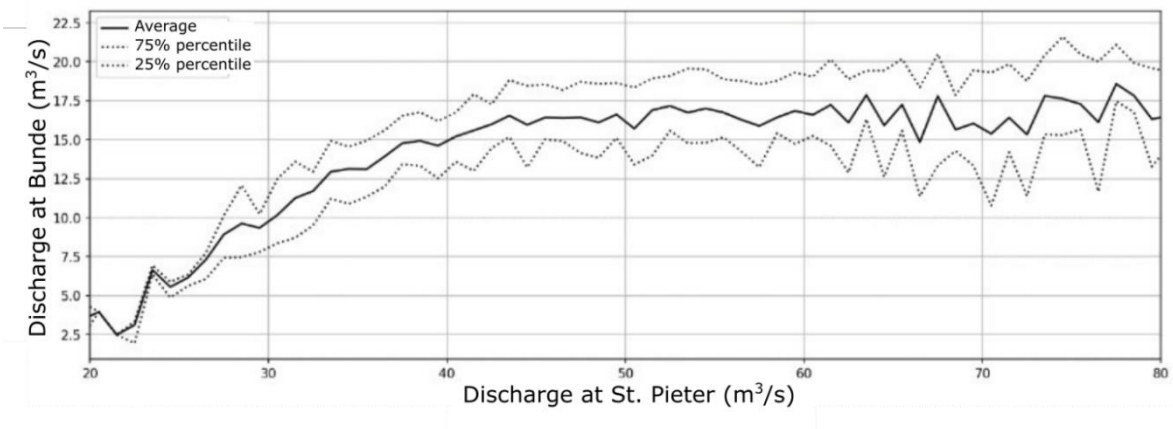

Figure 12: Analyses of discharge measurements from 1999 to 2018. The x-axis shows the discharge on the Meuse (at St. Pieter), the y-axis shows statistics (mean, and 25 % and 75 % percentile) of the discharge towards the locks (Julianakanaal at Bunde).

3.2 Method

To compute the water usage per strategy, the numerical model SIVAK is used to compute the number of levellings, supplemented with analytical models to calculate the corresponding water demand.

SIVAK III, developed by Systems Navigator for the Dutch government, is an agent-based model, where the lock operation (see Figure 13) is modelled for a given network (a lock complex with a few km of canal on both sides) and a given ship demand (all registered passages in a normative week). The model decides when levelling should be initiated based on three given criteria: actual

fill ratio of chamber with ships, potential fill ratio due to waiting ships at the other side of the lock, and a maximum waiting time for passing vessels. The outcome of the model is the passage time per ship and the number of levellings. By varying the levelling criteria, different outcomes are obtained.

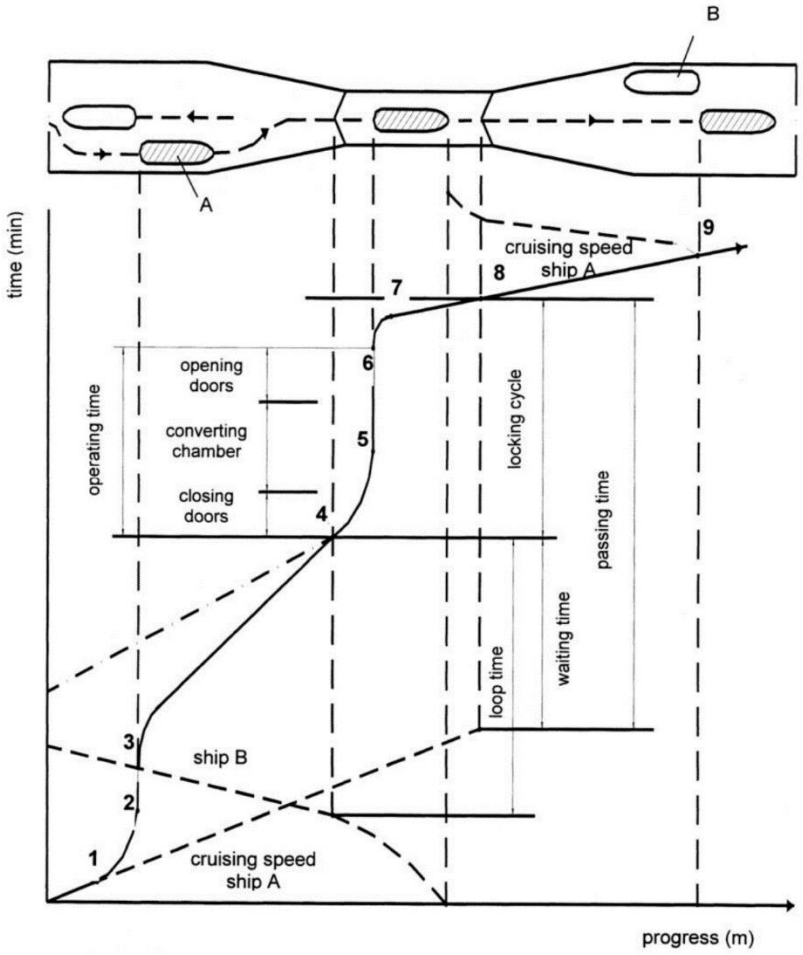

Figure 13: Space-time diagram of a levelling procedure [Groeneveld, 2006]

By post-processing these results[2], the costs in euros and the total water demand are calculated. The costs for the shipping sector are quantified by multiplying the additional waiting time with the costs per hour of that specific vessel type (on average 70 euro per hour, Panteia (2018)). The additional costs of operating the pumps varies between 0.004 and 0.005 euro per m^3.

Also, the water demand is computed by substantial post-processing. The levelling time from SIVAK cannot be combined with the effect of siphoning. Therefore, the exact times are computed with analytical models and linked to the model outcome. The basis of the levelling times is on observations, but this is alternated for siphoned levelling with the use of analytical models. This analytical model takes the dimensions of the siphons and basins, but also includes the criteria to which level the siphoning is operated.

3.3 Results

The results for three types of individual measures are given for the lock complex at Maasbracht in Figure 14. The figure shows the costs and discharge for the reference situation (green) and the effect of change in levelling regime, siphoning between locks and the use of pumps. It can be concluded that as a first measure to reduce water demand, pumps would be the most expensive

[2] Post-processing scripts available on **https://github.com/jurjendejong/pySIVAK**.

solution (the steepest line). The levelling regime is relatively cheap when going for a gentle regime, but when trying to save more water with a stricter regime if discharge drops further, the costs steeply increase. The siphoning is a relatively cheap solution and can save up to 6.5 m³/s.

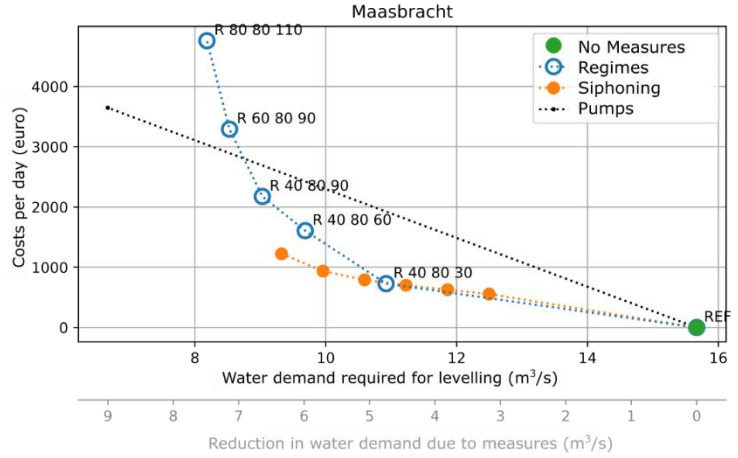

Figure 14: Effect of a levelling regime (blue), the use of siphoning between lock chambers (orange), or the use of pumps (black)

Based on those results a strategy with minimized costs is developed as given in Figure 15. The figure shows the discharge that is available for the locking process and the water that can be saved by using siphoning, levelling regime or pumps. The figure to the right gives the corresponding costs for these measures. In this strategy, at first the siphoning is fully activated resulting in higher costs for the shipping sector (longer passage times), for discharges lower than 9 m³/s the (gentle or strict regimes) are partly initialised, and for discharge below 6.5 m³/s the pumps are used for the additional savings among with more strict levelling regimes. The distinction between costs for the manager and for the shipping sector led to challenges in the optimisation. In the final result as given in Figure 15 the measures are chosen such that all costs above the dashed lined are split equally between both parties.

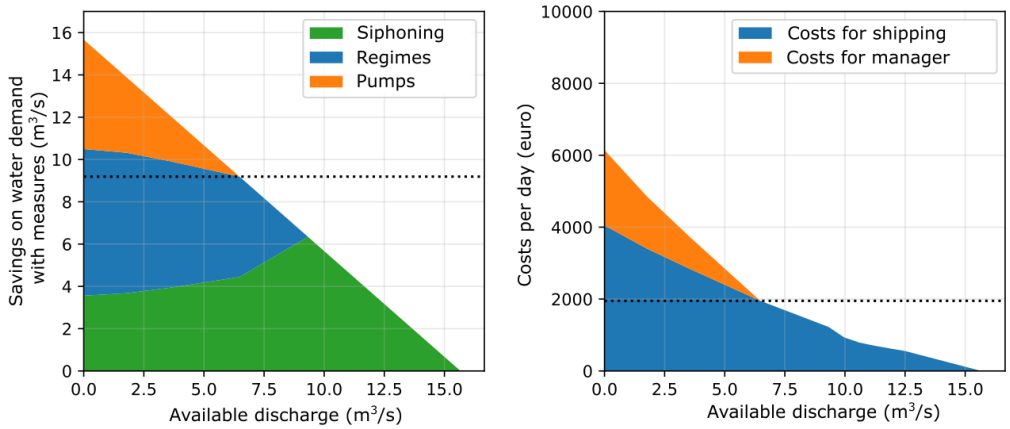

Figure 15: Water saving strategy for lock Maasbracht. For each available discharge (horizontal axes), water saving can be achieved by any of the three given measures: siphoning (green), levelling regimes (blue) and using pumps (orange). The right figure shows the resulting costs in this scenario, split by costs for the manager of the locks (orange) and for the shipping sector (blue).

Combining the discharge series for the climate scenarios with the costs at each discharge level, results in the total costs in those characteristic years as given in Figure 16. In very dry years in the current climate with a return period of 10 years, the additional costs due to drought are modelled at € 145,000, in the climate change scenario WH this increases to € 502,000. However, these years are very seldom and the average annual costs are lower: € 80,000 in the current climate and 230,000 in scenario Wh 2050.

Although these costs can be further lowered with infrastructural adjustments, the research showed that the required investments would probably be higher than the net present value of the savings.

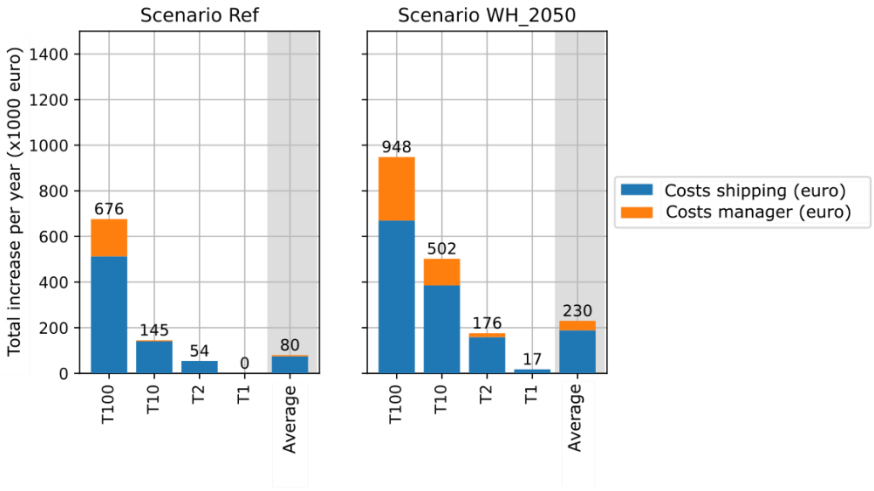

Figure 16: Additional costs at the lock at Maasbracht as a result of the drought with a return period of 100, 10, 2 and 1 year

4 STRESS TEST ON THE EFFECTS OF HIGH FLOW ON CLEARANCE HEIGHT

4.1 Introduction

The final stress test included in this paper, is research on limitations in clearance height during high flow conditions [Van der Wijk & De Jong, 2021]. The clearance height is used by container vessels to determine the number of layers of containers on their trip. During periods of higher discharge, the number of layers might need to be reduced as a result of low clearance height at one or multiple bridges along the route.

In this stress test it is evaluated which bridges on the route are most limiting in height. By combining this with discharges in different climate change scenarios and a dataset of all vessel types, it is calculated how often these bridges are limiting and for how many vessels.

4.2 Method

A dataset is used of all bridges over the Dutch rivers. The basis of this dataset is formed by the Fairway Information System (FIS)[3], but manual adjustments are performed to have a more accurate indication of the bridge height for each bridge.

Similar to the earlier stress tests, the basis of the analyses is formed from the time series of the daily-average discharge over 100 years. However, the statistical analysis is adjusted now to result in characteristic years for a given return period based on the years with the highest discharge.

For each discharge the water level at each bridge is calculated from a dataset of earlier performed model simulations (this product is called 'Betrekkingslijnen 2020-2021'). Subtracting the bridge height with the water level results in the available clearance height, as indicated in Figure 17.

[3] Publicly available on **https://vaarweginformatie.nl/**.

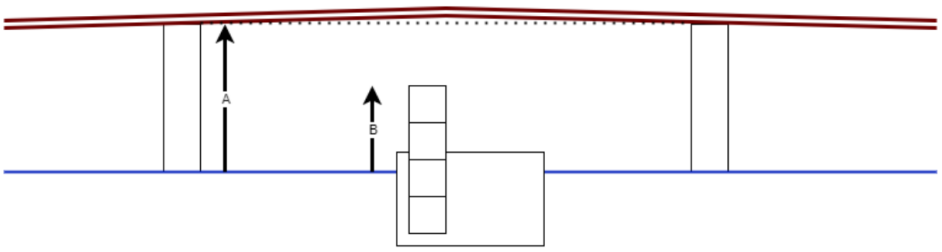

Figure 17: Sketch of a container vessel with 4 container layers under a bridge. Indicated with arrows are the available clearance height (A) and the required clearance height (B).

A vessel dataset is obtained from a model run on the annual IVS-registrations with BIVAS (see also earlier introduction in Section 2.2). For each bridge in the network, a query is performed to get a dataset of all vessels that passed this bridge over a year. The IVS registrations contain the number of containers per vessel but does not contain an accurate estimate of the height of the vessel and the number of layers of containers.

Using the formulae below, the containers per layer are estimated from the Length (L) and Width (W) of the container vessel. The total height of the vessel above water (H) can now be calculated based on the number of containers (n), the height per container layer of 2.896 m (Hn), the vessel's draught according to IVS (D), the vessels bottom thickness of 0.5 m (Hb) and a safety margin of 0.3 m (Hs). It should be noted that all these dimensions are based on the assumption that all containers are high cube containers. Although in practise many transported containers are still the conventional height of 2.59 m, the exact distribution is not known. By using high cube containers in the formulae, a conservative approach is used. An example of the distribution in container vessels on the Rhine at Nijmegen is shown in

Figure 18.

$$containers\ per\ layer\ = \frac{(0.9\ \cdot L - 10)}{6.2} \cdot \frac{W - 1.5}{2.45}$$

$$H\ = n \cdot H_n\ -\ D\ +\ H_b + H_s$$

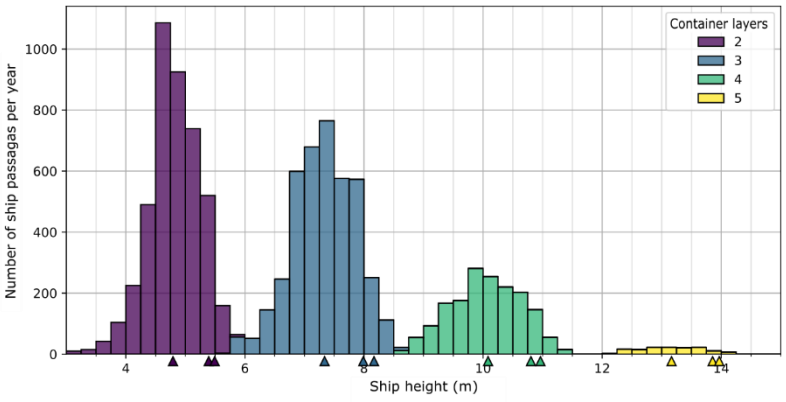

Figure 18: Distribution in ship height at Nijmegen (Rhine) based on the IVS data in BIVAS and the formulae above. The indicators on the x-axis mark the 50 %, 90 % and 95 % percentile of the height for the given number of container layers.

A model is set up where the distribution of required clearance height is compared to the available clearance height for a given river discharge in the climate change scenarios.

4.3 Results

The results of the clearance height analyses for the Rhine are summarised in
Figure 19. It shows the clearance height at the normative bridge on each branch of the Rhine. Typical heights that are often indicated as norms for container transport are 11.35 m and 9.1 m. In this figure we read that at the Prins Willem-Alexanderbrug on the river Waal, a height of 11.35 m is not available for 8 days a year, but that this might increase to 15 days due to climate change (scenario Wh 2085). During a year with a once-in-10-years high discharge, this height is not available for 22 days and this might increase to 32 days due to climate change. A height of 9.1 m is nearly always available on the Waal. However, on the river IJssel the available clearance height is substantially lower and is below 9.1 m for over 70 days per year in the current situation.

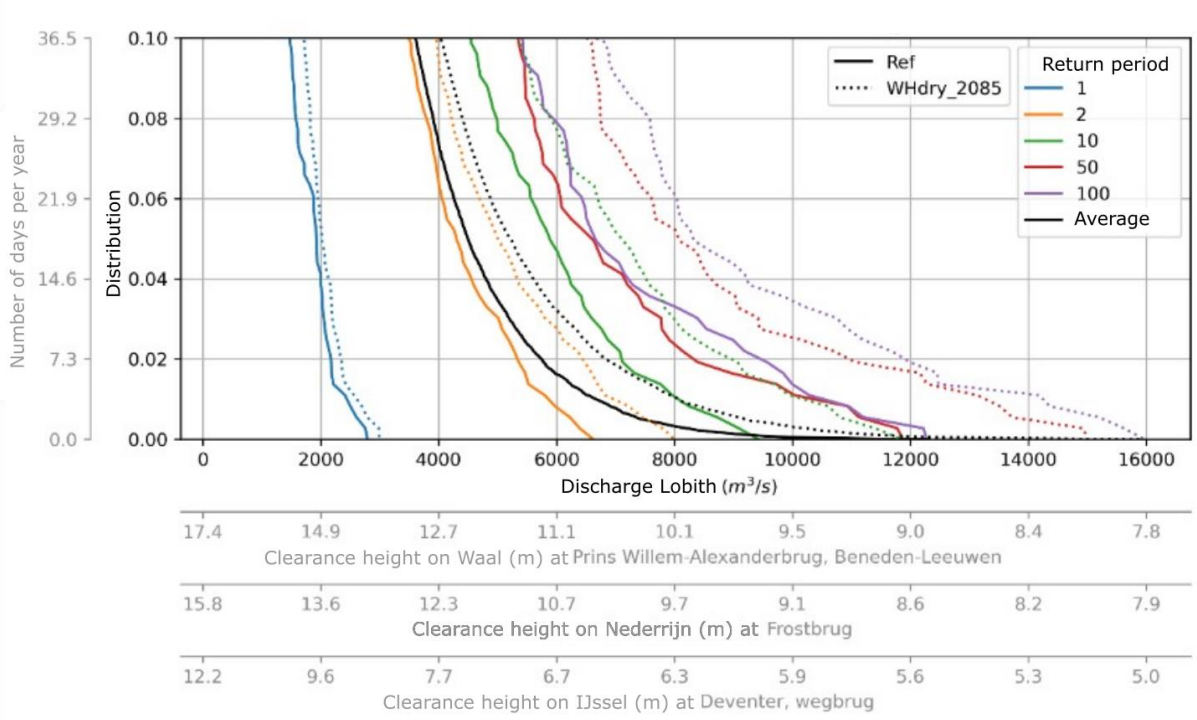

Figure 19: Distribution curve of the discharge on the Rhine at Lobith in an average year (black line) and in characteristic years with high discharge. For each discharge the secondary x-axis shows the bridge with the lowest clearance height on the major branches of the Rhine (respectively Waal, Nederrijn and IJssel).

By comparing the available height (

Figure 19) with the required height (

Figure 18) it is calculated how much the container transport is reduced as a result of the insufficient height. It is concluded that in an average year, the capacity is lowered by 1,300 TEU as a result of high discharge. This may increase to 2,200 TEU as a result of climate change (WH 2085). Compared to the total transport of 2 million TEU on the Waal this is approximately 0.1 %.

4.4 Discussion

The research shows that high discharge events only have impact on the number of container layers on a very limited number of vessels. In essence, the current standards for bridge height on the Rhine in the Netherlands result in such high bridges that the height of these bridges is hardly ever the limiting factor in the available clearance height. Nearly always, elsewhere on the route (i.e. outside the Netherlands) the bridges are lower. In many cases this involves the (lower) bridges on the Rhine in Germany. It is worthwhile to further discuss the necessity of the currently high bridge design standards [De Jong & Van der Wijk, 2021].

5 CONCLUSIONS

From the research on climate resilient infrastructure, it is concluded that climate change has the largest effect on the inland shipping on free-flowing river Rhine. The resulting risks and costs in the stress tests on clearance height and at locks are significantly lower. Although this is known from practise, the stress test has allowed to quantify the direct costs to the shipping sector as a result of the low flow. The annual costs from drought are calculated at 48 million in the current climate and an increase to 104 million as a result of climate change (scenario W_H in 2050). From an economic perspective it is important to know the year-to-year variation in costs. The costs in a year with probability of occurrence of once every 10 years, are calculated at 126 million in the current climate and can increase to 263 million as a result of climate change.

The reliability of the Rhine as a major transportation route is at stake. Considering the ambition of the European Union to increase the inland waterway transport, this poses a challenge to the realisation of a resilient fairway.

6 ACKNOWLEDGEMENTS

The study in this paper is carried out by a team of Deltares and under support of Rijkswaterstaat. As shown in the citations different stress tests were carried out with Rolien van der Mark, Remi van der Wijk and Tommaso Boschetti. The project was financed and lead by a team from

Rijkswaterstaat, a special thanks to Milou Wolters, Nathaly Dasburg, Roelof Weekhout, Pascal Witmer and Frederik Vinke. The applied methods and reports are the result of an intensive collaboration between Deltares and Rijkswaterstaat.

7 REFERENCES

Groeneveld (2006): "Capacities of Inland Waterways", Lecture Notes TU Delft CT 5306.

Jong, J.S. de (2019a): "KBN: Bedreiging klimaatverandering – Beschrijving karakteristieke droge jaren met stationaire afvoerniveaus", Deltares memo 11203738-005-BGS-0002 versie 1.1, d.d. 14 december 2019 (in Dutch).

Jong, J.S. de (2020a): "KBN – Stresstest droogte Maas – Bedreiging: Klimaatverandering. Beschrijving karakteristieke droge jaren met stationaire afvoerniveaus", Deltares memo 11205274-004-BGS-0003 d.d. 18 juli 2020 (in Dutch).

Jong, J.S. de (2020b). Stresstest Droogte Rijntakken – Impact op de scheepvaart. Technical report, Deltares v1.1, kenmerk 11205274-004-BGS-0009 (in Dutch).

Jong, J.S. de and Mark, R. van der (2021): "KBN-HVWN Stresstest droogte Rijntakken: Toestand van het Systeem en Kwetsbaarheid gebruiksfunctie", Technical report, Deltares 11205274-004-BGS-0022 v1.1, d.d. 7 mei 2021 (in Dutch).

Jong, J.S. and Boschetti, T. (2021): "Kwetsbaarheid sluizen Maas voor klimaatverandering. Onderzoek naar de sluizen Born, Maasbracht en Heel in klimaatbestendige netwerken", Technical report, Deltares 1120527-004-BGS-0017 v1.0 d.d. 19 april 2021 (in Dutch).

Jong, J.S. de and Wijk, R. van der (2021): "Discussie over de normering van de doorvaarthoogte in Nederland, in relatie tot de normering in Duitsland en de gewenste doorvaarthoogte", Technical memo, Deltares 11206832-019-GEO-0001, d.d. 15 november 2021 (in Dutch).

Koedijk, O.C. (2020): "Richtlijnen vaarwegen 2020", Tech. rep., Ministerie van Infrastructuur en Waterstaat, Rijkswaterstaat Water, Verkeer en Leefomgeving (in Dutch).

KNMI (2015): "KNMI'14 Climate Scenarios for the Netherlands", KNMI, De Bilt, the Netherlands, 34 pp.

Panteia (2018): "Kostengetallen binnenvaart 2017 – methodologie" (in Dutch).

Sloff, K. (2019): "Prognose bodemligging Rijntakken 2020-2050. Trends voor scheepvaart en waterbeschikbaarheid", Technical report, Deltares 11203738-005-BGS-0008 (in Dutch).

Wijk, R. van der & Jong, J.S de (2021): "Stresstest Doorvaarthoogte Hoofdvaarwegennet. Zeespiegelstijging en rivierafvoeren", Technical report, Deltares 11205274-004-BGS-0023 v8.0, d.d. 30 augustus 2021 (in Dutch).

Ylla Arbós, C., Blom, A., Vuren, S. van, Schielen, R.M.J. (2019): "Bed Level Change in the Upper Rhine Delta since 1926 and Rough Extrapolation to 2050", Delft University, November 2019.

SUMMARY

In a series of stress tests, the robustness of the inland waterway transport infrastructure within the Netherlands to climate change is studied. The performance of the system under low flow and

high flow conditions results in (1) lower available draught due to limited water depth, (2) longer levelling time due to insufficient water availability at locks, and (3) a lower number of container layers due to limitations in the clearance height at bridges. For inland shipping in the Netherlands, the stress test on the limitations on draught showed to have the largest economic consequences to the costs of transport over water.

RESUME

Une série de tests de stress a permis d'étudier la robustesse de l'infrastructure de transport fluvial aux Pays-Bas face au changement climatique. Les performances du système dans des conditions de débit faible et élevé se traduisent par (1) un tirant d'eau disponible plus faible en raison d'une profondeur d'eau limitée, (2) un temps de nivellement plus long en raison d'une disponibilité d'eau insuffisante aux écluses, et (3) un nombre plus faible de couches de conteneurs en raison de la limitation de la hauteur de dégagement aux ponts. Pour la navigation intérieure aux Pays-Bas, le test de stress sur les limitations du tirant d'eau s'est avéré avoir les conséquences économiques les plus importantes sur les coûts du transport par voie d'eau.

ZUSAMMENFASSUNG

In einer Reihe von Stresstests wird die Robustheit der Binnenschifffahrtsinfrastruktur in den Niederlanden gegenüber dem Klimawandel untersucht. Die Leistung des Systems bei Niedrig- und Hochwasser führt zu (1) einem geringeren verfügbaren Tiefgang aufgrund begrenzter Wassertiefe, (2) einer längeren Nivellierungszeit aufgrund unzureichender Wasserverfügbarkeit an Schleusen und (3) einer geringeren Anzahl von Containerlagen aufgrund von Einschränkungen der Durchfahrtshöhe an Brücken. Für die Binnenschifffahrt in den Niederlanden hat der Stresstest zu den Tiefgangsbeschränkungen die größten wirtschaftlichen Auswirkungen auf die Kosten der Beförderung auf dem Wasser.

RESUMEN

En una serie de pruebas de resistencia, se estudia la solidez de la infraestructura de transporte por vías navegables interiores de los Países Bajos frente al cambio climático. El comportamiento del sistema en condiciones de bajo y alto caudal se traduce en (1) un menor calado disponible debido a la limitada profundidad del agua, (2) un mayor tiempo de nivelación debido a la insuficiente disponibilidad de agua en las esclusas, y (3) un menor número de capas de contenedores debido a las limitaciones en la altura libre en los puentes. Para la navegación interior en los Países Bajos, la prueba de resistencia a las limitaciones de calado demostró tener las mayores consecuencias económicas para los costes del transporte por agua.

PIANC De Paepe-Willems Award 2023 – Second Place

DAMAGE PROGRESSION MODEL FOR DAMAGE ACCUMULATION IN RIPRAP REVETMENTS AT ARTIFICIAL INLAND WATERWAYS

Julia Sorgatz

During the research: Researcher/advisor river dynamics and inland shipping at Deltares, P.O. Box 177 2600 MH Delft, the Netherlands

Jurjendejong@gmail.com

8 INTRODUCTION

To promote inland shipping as a sustainable and efficient transport mode, it is required to provide a waterway infrastructure which allows for a broad navigability of larger or more powerful vessels. Yet, under increasing economic and ecological pressures, an integral analysis of revetment stability over the entire life cycle is aimed for in order to minimise costs while securing the current level of safety. For this purpose, it is essential to understand and to predict the deterioration and failure of bank revetments.

Revetments are commonly built of an erosion-resistant armour stone layer, a filter layer and below, if necessary, a sealing layer. Most frequently, technical bank revetments are installed which secure the bank from the bottom of the river or canal to the highest possible wave emergence [MAR, 2008]. There are various types of cover layers, the installation of which depends in particular on the expected loads (see Figure 1). The presented investigations focus on riprap revetments.

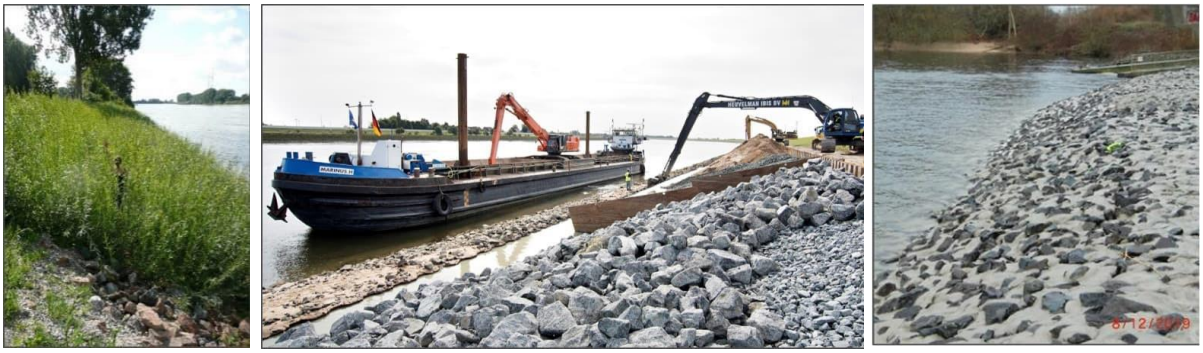

Figure 1: Different types of bank protections at inland waterways: technical-biological bank revetments, riprap revetments and grouted armour stone revetments (Photos: BAWArchiv)

Damage of riprap revetments is a result of unbalanced loads and resistances often caused by a combination of unfavourable circumstances, e. g., poor installation, ships passing too close to the bank or excessive speed [PIANC, 1987 ; USACE, 1997 ; Fleischer and Kayser, 2006 ; Rock Manual, 2007 ; Uliczka et al., 2018]. From expert interviews [Sorgatz, 2021], it was derived that from the point of maintenance armour stone displacement is the most significant type of damage along inland waterways.
In the past, damage progression of rock armour layers on non- and marginally overtopped structures was investigated by small-scale tests [Hudson, 1958, 1959 ; Font, 1968, 1970 ; Thompson and Shuttler, 1975 ; Pilarczyk and den Boer, 1983 ; Pitt and Ackers, 1983 ; van der Meer and Pilarczyk, 1984 ; Lee et al., 1987 ; Verheij and Bogaerts, 1989 ; Daemrich et al., 1996 ; DST, 2006; Hofland et al., 2014 ; Uliczka et al., 2018] and large-scale experiments [Ahrens, 1970 ; van der Meer and Pilarczyk, 1984 ; Köhler, 1985 ; Bezuijen et al., 1987 ; van der Meer, 1987 ; Westrich, 2003 ; Gier, 2017 ; Kreyenschulte, 2020]. These investigations predominantly resulted in design approaches for breakwaters and other coastal structures, i.e. the definition of design formulae that refer to specific revetment conditions ('point of failure'). Although, it must be noted that this 'point of failure' differs between different authors [Medina, 1992].

Few studies are concerned with damage evolution, which are, however, bound to certain constructions or boundary conditions that represent breakwaters and other coastal protection structures, e.g. [Melby and Kobayashi, 1998a, 1998b ; van der Meer, 2000 ; Melby, 2001 ; Hofland et al., 2018]. For instance, the formulae by van der Meer (1987, 2000) are applicable to the calculation of equivalent and cumulative damage for large storm events where each storm event is characterised by a set of wave parameters such as breaker type or significant wave height. The damage progression model by Melby (2001) is calibrated for storm events with large wave heights

at breakwaters with a slope inclination of 1*V*:2*H*. On inland waterways, however, an exceedance of the limit state occurs less frequently only if a vessel passes the shore closer or faster than anticipated by design. Moreover, on inland waterways the design wave heights and, thus, the armour stones are smaller.

In this paper, a damage progression model applicable to riprap revetments at artificial inland waterways is presented. For this purpose, firstly, a series of full-scale model tests is conducted. During these tests, the damage progression is assessed by successive laser scans. Subsequently, different damage indicators and their correlations are evaluated using the experimental data. Then, the damage progression model developed by Castillo et al. (2012) is modified and calibrated for different damage indicators and the conditions at artificial inland waterways.

The paper is organised as follows: in Section 2, typical damage indicators, damage progression models and failure definitions are introduced. Section 3 presents the experimental set-up of a full-scale embankment model which was repeatedly loaded with waves. The experimental results are presented in Section 4. To evaluate their validity and their applicability to existing damage progression models, the results are compared to data from literature. In Section 5, the modified damage progression formulae, the calibration process and results are presented. In Section 6, methodology and findings are discussed. Finally, this paper closes with a brief recap of results and an outlook regarding future research.

2 DAMAGE OF RIPRAP REVETMENTS

2.1 Damage Indicators

According to PIANC (2003), there a three different types of armour layers: non-reshaping statically stable structures where only few armour stones are allowed to move, reshaped, now statically stable structures where the structure's profile is allowed to change into a stable profile and the position of individual armour stones is stable and dynamically stable reshaping structures where the profile is reshaped into a stable profile, but individual armour stones can still move. This paper deals with non-reshaping statically stable structures.

The degree of damage can be characterised by visual classification [Hedar, 1965 ; Kayser, 2015 ; Sorgatz et al., 2018], by the number of eroded stones [Hudson, 1959 ; van de Kreeke, 1969 ; Font, 1970 ; Ouellet, 1972 ; Thompson and Shuttler, 1975], in relation to an eroded area [Pilarczyk and den Boer, 1983 ; van der Meer, 1988 ; Melby, 1999] or in relation to the eroded volume [Broderick, 1983]. The condition of statically stable rock structures is typically characterised by damage numbers, which, in turn, are related to number, area or volume of eroded armour stones.

The oldest quantitative damage measure is the number of displaced armour stone units, N_{od} or the number of displaced armour stone units N_d within a strip of the width of the nominal armour stone diameter D_n [Hudson, 1959 ; van de Kreeke, 1969 ; Font, 1970]:

$$N_{od} = \frac{number\ of\ units\ displaced\ out\ of\ armour\ layer}{width\ of\ tested\ section} \tag{1}$$

$$N_d = \frac{number\ of\ units\ displaced\ out\ of\ armour\ layer}{total\ number\ of\ units\ within\ reference\ area/D_n} \tag{2}$$

A major shortcoming of this damage classification is its applicability in the field as the armour stones usually roll off the embankment towards the toe and thus cannot be counted. Therefore, measures were proposed that are based on the surface profile of a (simple) slope. When the

erosion area around still water level is related to the size of the rocks, a dimensionless damage level is obtained which is independent of the size (slope angle and height) of the structure [Broderick, 1983 ; Pilarczyk and den Boer, 1983]. This dimensionless damage level *S* is defined by:

$$S = \frac{A_e}{D_{n50}^2} \tag{3}$$

where A_e is the eroded area and D_{n50} is the mean nominal armour stone diameter. In addition to *S*, [Melby and Kobayashi, 1998a] introduce the dimensionless damage depth *E*, the normalised cover depth *C* and the normalised eroded length *L* to account for the shape of the eroded region:

$$E = \frac{d_e}{D_{n50}} \tag{4}$$

$$C = \frac{d_c}{D_{n50}} \tag{5}$$

$$L = \frac{l_e}{D_{n50}} \tag{6}$$

where d_e defines the maximum slope-normal distance between the undamaged and damaged profiles, d_c is the cover depth and l_e is the eroded length (see Figure 2). Throughout this paper, the averages of the damage indicators ($\bar{S}$, E, $\bar{C}$ and L) computed for a specific test section are used (see also Section 3.2).

2.2 Damage Development

Revetment stability for regular and irregular wave attack have been studied by many researchers over the past years [Iribarren, 1949 ; Iribarren and Nogales, 1951, 1952 ; Hudson, 1958, 1959 ; Font, 1968, 1970 ; Ahrens, 1970 ; Thompson and Shuttler, 1975 ; Pilarczyk and den Boer, 1983 ; Pitt and Ackers, 1983 ; van der Meer and Pilarczyk, 1984 ; Bezuijen et al., 1987 ; Lee et al., 1987 ; van der Meer, 1987 ; Verheij and Bogaerts, 1989 ; Daemrich et al., 1996 ; Melby and Kobayashi, 1998a, 1998b ; van der Meer, 2000 ; Melby, 2001 ; DST, 2006 ; Hofland et al., 2018]. Yet, only few studies are concerned with damage evolution models, e.g. Melby and Kobayashi (1998a, 1998b), van der Meer (2000), Melby (2001) and Hofland et al. (2018). Three well-known damage progression models are presented below.

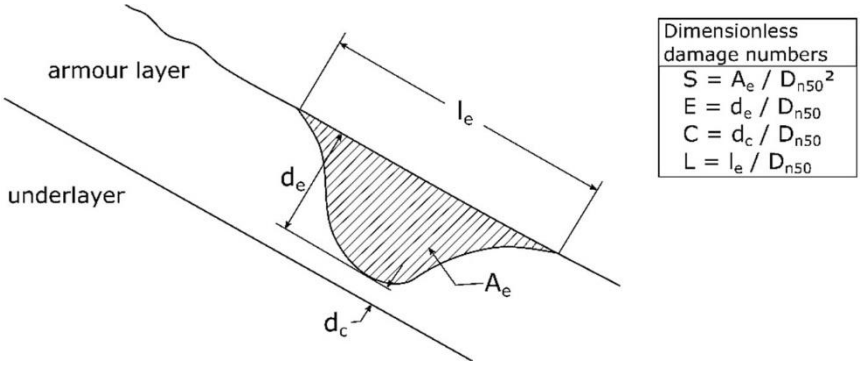

Figure 2: Dimensionless damage numbers. Illustration based on Melby and Kobayashi (1998a).

Based on his design formulae for riprap revetments [van de Meer, 1987], van der Meer (2000) described a method to account for cumulative damage by calculating equivalent damage for different storm events and the corresponding number of waves to reach this equivalent damage per storm event. The damage progression depends on wave characteristics such as significant wave height, wave period, breaker type and the number of waves, on the properties of the

structure such as geometry and armour stone density, and on empirical coefficients. Based on an equivalent damage, the cumulative damage is determined.

A major contribution to damage development formulae was presented by Melby and Kobayashi (1998a, 1998b) and Melby (2001). They give a mathematical description of progressive damage due to the occurrence of subsequent storm events in terms of cumulative damage S allowing for non-zero initial damage. The Melby equation is based on van der Meer (1987) design formulae, but simplifies them by introducing additional empirical factors:

$$S(t_n) = S(t_0) + 0.025 \frac{N_{s,n}^5}{T_{m,n}^5} \left(t_n^b - t_0^b\right) \tag{7}$$

where N_S is the stability number, T_m the mean wave period, t_n the duration of the storm event, t_0 the duration time of a storm to reach a damage level $S(t_0)$, $S(t_n)$ the damage at time t_n, $S(t_0)$ the damage at time t_0, n a time counter and b an empirical coefficient (commonly b = 0.25).

Riprap stability is highly variable, and stochastic in nature, as both the loading [Scotto and Guedes-Soares, 2007] and the riprap conditions are. Castillo et al. (2012) thus proposed a dimensionless stochastic damage progression model (DDPM). The model is based on dimensional analyses, compatibility conditions and the central limit theory. Instead of selecting easy to use mathematical functions, a mathematical formulation was chosen which satisfies a set of properties. It is applicable to different damage indicators. It is expressed in terms of a cumulative density function F of the dimensionless damage D^*:

$$F_{D^*(t^*)}(x) = \Phi\left(\frac{(x-\gamma)^{\frac{1}{b}} - \mu_0 - kt^*}{\sqrt{\sigma_0^2 + rt^*}}\right) \tag{8}$$

where $\Phi(x)$ is the cumulative density function of a standard Gaussian distribution, $t^* = {}^{tn}/_{\mathrm{Tm}}$ is the number of waves as a result of load duration t_n and mean wave period T_m, γ and b are breakwater dependent coefficients, k and r are empirical coefficients that account for the wave action and μ_0 and σ_0 are mean and standard deviation of the initial damage or the initial condition of the revetment. Any dimensionless damage indicator can be used for D^*.

2.3 Failure Definition

A key information to be derived or predicted based on data on the damage indicators over time is the point of failure. Hofland et al. (2013, 2014, 2018) suggested a classification of the damage severity for structures with a $2\,D_{n50}$ thick armour layer where E = 0.2 - 0.3 is considered as initial damage and E = 0.5-0.6 is classified as intermediate damage and failure is defined as the exposure of the filter layer with E = 0.8-1.6. In the Rock Manual (2007) the failure of a 1:3 slope is indicated by S = 12. Melby and Kobayashi (1998a, 1998b) give the following equation for the mean damage S at failure initiation:

$$0.1\,S + 2.7\,[0.098 - 0.002\,(S - 7)^2] = C - 2.7\,\sigma_{C_0} \tag{9}$$

The formula indicates that the damage at the time of failure depends on the initial cover layer thickness expressed via the initial normalized cover depth C as well as on its initial variability σ_{C_0} which can be interpreted as a measure of 'smoothness' of the revetment after construction. In the case of the three test series by Melby and Kobayashi (1998a), eq. (9) yields a failure point ranging between

S = 5.4-10.9. However, it must be noted that σ_{C_0} is a function of the cove layer thickness and armour stone size. It must thus be assessed specifically for different cover layers.

At artificial inland waterways the displacement of few armour stones does not immediately lead to slope failure. However, since a change in the hazard situation is not up to discussion, great attention must be directed to revetment conditions that impose a risk to the embankments' functionality. In this paper, failure refers to a condition of the structure where the soil of the embankment is no longer sufficiently protected against erosion [Sorgatz, 2021]. Failure is thus defined as the point at which less than one layer of armour stones covers the embankment ($\overline{C}$ between 1-1.5, C_0 - Ē between 1-1.5).

3 MODEL TESTS

3.1 Experimental Set-Up

3.1.1 Geometry

Figure 3 gives an impression of the different stages of the construction of the embankment model. For the herein presented model tests, a full-scale embankment model secured by loose armour stone revetment is built in a wave basin of the size 8 m x 14 m x 6 m (*B* x *L* x *T*). The slope inclination amounts to 1*V*:3*H*. The embankment material is characterised as a medium fine sand with a hydraulic conductivity of $k_f \approx 1 \cdot 10^{-4}$ m/s. The sand is placed and compacted in layers of 0.20 m. Compaction and bulk density are controlled during placement with dynamic load plate tests and densitometer tests. The two- stage granular filter has a thickness of 2 x 0.15 m and is secured by loose armour stones of the length class CP45/125 [TLW, 2003]. The armour stones are narrowly graded with a median mass *M*50 = 1.11 kg, a mean nominal diameter D_{n50} = 64.50 mm and an armour stone density ρ_s = 2650.00 kg/m³. The underlying filter layer is design according to MAK (2013) and MMB (2013). Despite the slightly smaller armour stones than average, the embankment model can be considered as a standard structure built at German inland waterways. A cross-sectional and longitudinal view of the wave basin is given in Figure 4.

3.1.2 Measurement Devices

Except from the pore pressure sensors all measurement devices used throughout the tests are shown in Figure 4 and Figure 5. The wave heights are gauged with the aid of four ultrasonic sensors (US) in the direction of the slope. Additionally, four capacitive wave height devices (Harfe) are attached to the bridge on top of the wave basin. Flow velocities are detected in two cross-sections on the revetment surface by two inductive flow velocity metres (ISM). Potentially occurring excess pore pressure in the ground is monitored by twelve absolute pressure transducers (PR) which are installed in two cross- sections at different depths (see Figure 4). Additionally, the two pressure transducers directly below the filter layer are used to validate the wave heights



measured by ultrasonic sensors and the capacitive wave height devices. The armour stone displacements are observed by subsequent laser scans.

Figure 3: Impressions of the wave basin construction: (a) slope with filter layer, (b) slope with armour stones; the pipes indicate the position of pore pressure sensors in the ground; (c) wave basin filled with water shortly before the start of the trial (Photos: Sorgatz)

Figure 4: Cross-sectional and longitudinal view of the wave basin

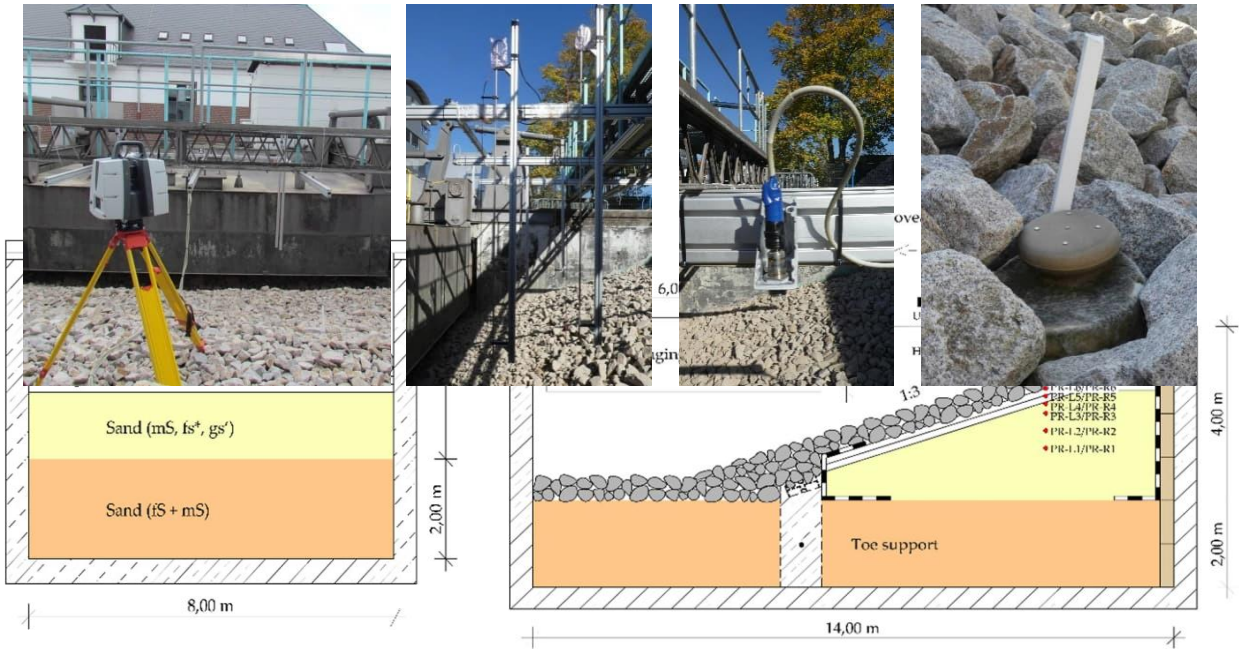

Figure 5: (a) Laser scanner, (b) wave height devices (Harfe), (c) ultrasonic sensors (US) and (d) inductive flow velocity metres (ISM) (Photos: Sorgatz)

4 TEST PROCEDURE AND DATA ANALYSES

4.1 Wave Loading

The waves are generated by a partially submerged plunging body at the lower end of the slope (see Figure 4). In each test, a total of 50 waves is generated by 50 fast, regular lifting movements of the plunging body. The lifting movement of the plunging body results in an orthogonal wave and a back-flow of water after wave breakage. Following the wave exposure, the water is drained from the wave basin and the armour stone displacement is recorded. The described procedure of wave loading, water drainage and revetment scanning is repeated several times. In total, two test series are conducted (see Table 1). The number of tests varies between the different series as one important requirement of the test series was that the slope stability is not endangered during testing.

		H_S in m			T_m in s			t_n in s		
		Harfe 1	*Harfe 3*	Mean	*Harfe 1*	*Harfe 3*	Mean	*Harfe 1*	*Harfe 3*	Mean
Series 1	Test 18/0 [1]	--	--	--	--	--	--	--	--	--
	Test 18/1	0.26	0.25	0.26	4.03	4.02	4.02	189.252	188.81	189.03
	Test 18/2	0.24	0.20	0.22	3.99	4.00	4.00	191.357	192.24	191.80
	Test 18/3	0.25	0.22	0.24	4.45	4.47	4.46	151.337	152.05	151.69
	Test 18/4	0.26	0.22	0.24	4.00	4.01	4.01	200.215	200.29	200.25
Series 2	Test 19/0 [1]	--	--	--	--	--	--	--	--	--
	Test 19/1	0.23	0.20	0.21	3.91	3.93	3.92	195.54	196.34	195.94
	Test 19/2	0.25	0.24	0.24	3.81	3.89	3.85	202.13	202.22	202.17
	Test 19/3	0.24	0.22	0.23	3.92	3.87	3.90	199.75	201.44	200.60
	Test 19/4	0.27	0.23	0.25	3.67	3.21	3.44	205.78	205.61	205.70
	Test 19/5	0.22	0.19	0.21	4.37	4.18	4.27	188.06	196.3	192.18
	Test 19/6	0.27	0.23	0.25	3.90	3.62	3.76	202.55	202.57	202.56
	Test 19/7	0.22	0.20	0.21	3.99	3.84	3.91	191.38	192.04	191.71
	Mean μ	0.25	0.22	0.23	4.00	3.91	3.96	192.49	193.63	193.06
	Std σ	0.02	0.02	0.02	0.23	0.32	0.26	14.9	14.74	14.77

[1] initial measurement

Table 1: Design parameters for the assessment of damage progression: significant wave height H_S, mean wave period T_m and the load duration t_n

To assess the damage development, the significant wave height H_s as well as the mean wave period T_m and the load duration t_n are gathered from the wave measurements (see Table 1). H_s is computed as the average wave height, from toe to crest, of the highest one-third of the waves. Although the wave heights are recorded redundantly by different devices, only selected measurements (*Harfe 1* and *Harfe 3*) are presented herein. The additional measurement devices are used to validate the presented data.

Overall, it is observed that the mean values of H_s, T_m and t_n differ only slightly between the left and right cross-section of the wave basin as well as between the individual tests. Small standard deviations (std / σ) confirms this observation. N_s ranges between 1.94 and 2.40 with a mean value μ = 2.17 and a standard deviation σ = 0.15. According to Rock Manual (2007) the stability number N_s ranges between 1 and 4 for statically stable structures. Consequently, it is confirmed that the following evaluations are limited to statically stable structures.

4.1.1 Armour Stone Displacements

The armour stone displacements are observed by subsequent laser scans. This method has already been used by other authors for comparable tasks indoors (the wave basin is an outdoor location, see also Section 5). It is characterized by a high accuracy, e.g. Schendel et al. (2016), Shen et al. (2017) and Hofland et al. (2018). The scanner generated a three-dimensional point cloud of the revetment and the wave basin. Measurement accuracies caused by different levels of brightness as discussed in Shen et al. (2017) are reduced by scanning the wave basin one day after drainage at the earliest. The use of four different scan positions allows to detect hidden edges of the armour stones. A local coordinate system is used to superimpose several scans for the identification of areas of armour stone displacements in a height difference model. The individual scans are recorded with a high resolution resulting in large datasets. Post- processing is therefore indispensable for further evaluation (see Figure 6).

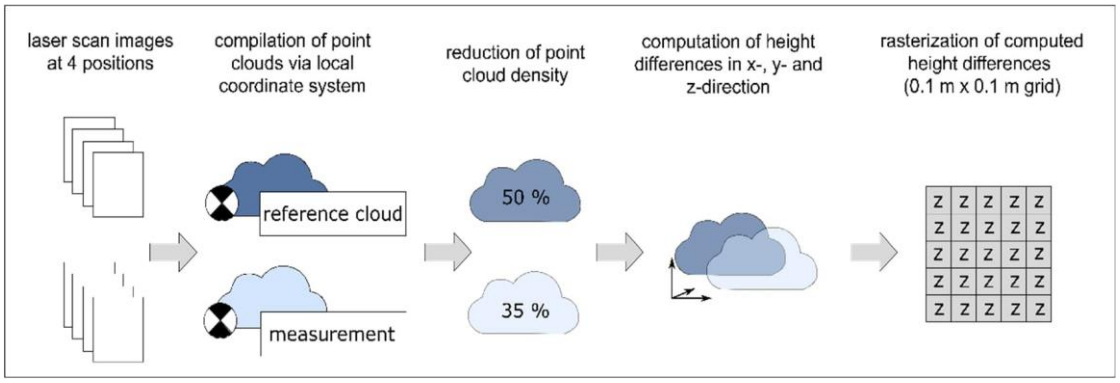

Figure 6: Illustration of the post-processing of the point clouds

The height differences are computed between the reference cloud (see Table 1, initial measurement) and each measurement within one test series. During post-processing the point cloud density is reduced to obtain a homogeneous point cloud density over the entire model on the one hand, while reducing the computational effort on the other hand. In order to achieve a high quality comparison between the point clouds, the reference point cloud (initial conditions) is reduced to 50 % of the initial point cloud density, whereas the ensuing measurements are reduced to 35 % of the initial point cloud density.

Subsequently, the height differences are determined with the software package CloudCompare [Cloud Compare, 2018] divided into an x-, y- and z-component. Based on preliminary examinations, a 2D1/2 triangular local modelling with 12 points is chosen for the computation. This procedure projects the point cloud in 2-D on the XY plane. Then, the corresponding 2-D points are triangulated and a mesh structure is applied to the 3-D points. The computed height differences are then analysed with respect to the z-component which represents the armour stone displacement in vertical direction. For a comparison of the individual test series amongst each other, the computed z-differences were rasterized on a 0.100 m x 0.100 m grid.

5 EXPERIMENTAL RESULTS

5.1 Current Test Series

Unlike conventional measurements, e.g. hand sounding and depth measurement with folding rule, the laser scanner allows for a spatial and a cross-sectional analysis of the revetment condition. The temporal and spatial damage evolution of the entire surface under wave loading is shown in Figure 7 and Figure 8. In Figure 7, the black shaded areas indicate erosion, whereas the red shaded areas indicate material aggregation. It is observed that the armour stones move from the area of water fluctuation towards the toe of the embankment. The centre and left area of the wave basin are more strongly affected by armour stone displacements than the right area. This is probably due to a slight misalignment of the plunging body. However, for now, the effects on the further analyses are assumed to be negligible.

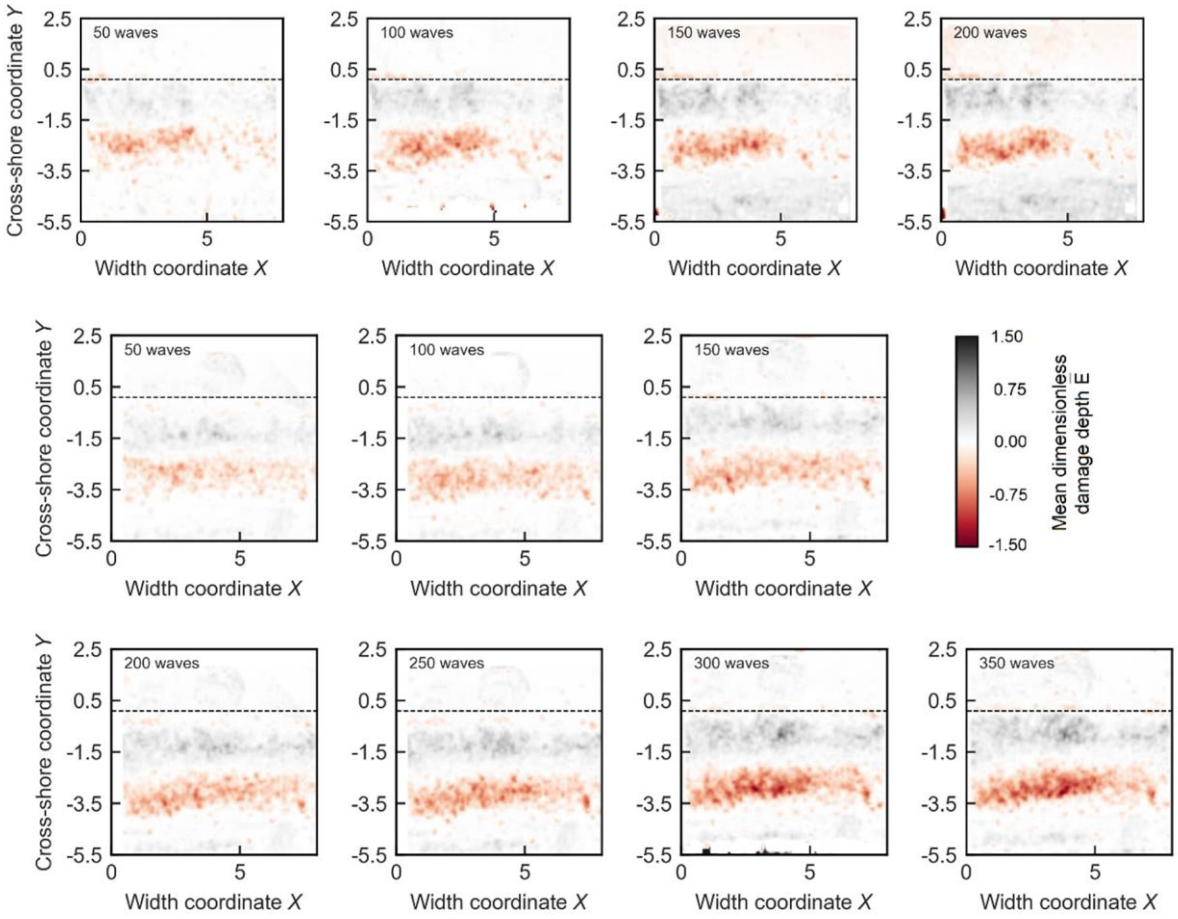

Figure 7: Spatial development of the damage evolution with increasing wave loading. The origin of the cross- shore coordinate Y is the waterline. The top edge of the slope is indicated by the dashed line.

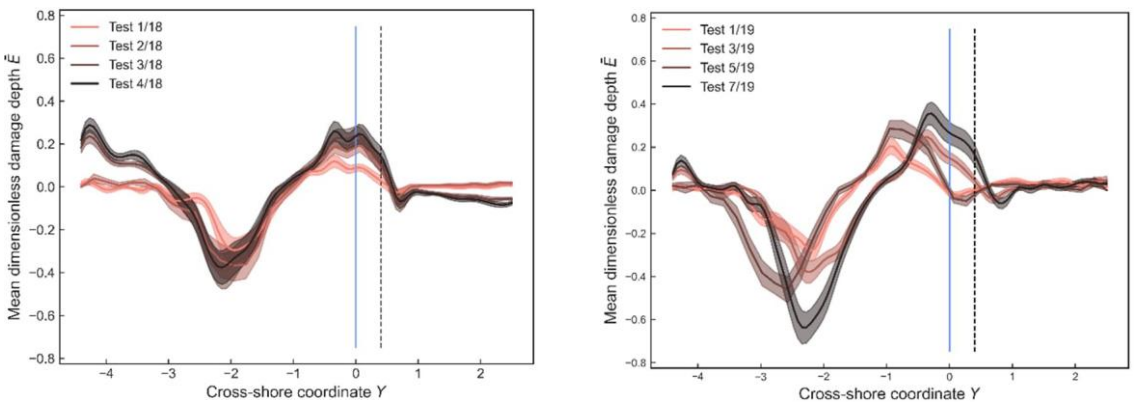

Figure 8: Width-averaged erosion profiles over time with confidence bands (shaded areas). The origin of the cross-shore coordinate Y is the waterline as indicated by the solid line. The top edge of the slope is indicated by the dashed line. For the sake of clarity, only every second test is shown for Series 2.

The variance of the erosion across the width of the wave basin is shown in Figure 8 by the confidence bands of the mean (shaded areas) in the width-averaged erosion profiles over time. To compute mean and confidence bands, the entire width of the rasterized wave basin is used. Both *Series 1* and *Series 2* show a similar damage progression. Moreover, the figures indicate that the top edge of the slope, which is marked by the dashed line, steepens with each loading cycle and moves in inland direction. A typical S-shaped profile develops.

To provide more accurate information on damage development the damage numbers are evaluated along three prominent profiles (see Table 2). In accordance with the definitions of the damage numbers, the analyses focuses on the upper black coloured area ranging between -2.0 ≤ *Y* ≤ 0.5 (area of water level fluctuation). $\bar{S}$ is calculated by summing the products of depth x grid size over the specific cross-section. $\bar{E}$ and $\bar{C}$ are calculated from the maximum erosion depth determined in an area of 0.100 m x 0.100 m. $\bar{L}$ is calculated from the difference of the beginning and the end of the erosion zone times the width of the wave basin. To reduce the significance of outliers, Table 2 shows the mean value of 10 grid cells per cross section corresponding to 1 m in the real-world model.

		Mean damage level $\bar{S}$			Mean damage depth $\bar{E}$			Mean cover depth $\bar{C}$			Mean damage length $\bar{L}$		
		Left	Centre	Right	Left	Centre	Right	Left	Centre	Right	Left	Centre	Right
Series 1	Test 18/1	2.12	2.35	0.48	0.27	0.3	0.15	7.48	7.47	7.59	12.01	11.63	2.31
	Test 18/2	4.12	4.7	1.31	0.47	0.48	0.24	7.34	7.33	7.5	18.62	17.7	7.04
	Test 18/3	5.43	5.13	1.33	0.61	0.53	0.26	7.23	7.28	7.49	19.86	17.24	5.96
	Test 18/4	5.49	5.93	1.57	0.62	0.6	0.26	7.22	7.24	7.48	19.09	23.09	6.54
Series 2	Test 19/1	2.21	3.38	1.13	0.32	0.44	0.23	7.47	7.34	7.52	15.91	29.93	16.16
	Test 19/2	2.77	3.79	1.36	0.41	0.52	0.27	7.39	7.29	7.5	15.39	13.85	NA
	Test 19/3	2.85	4.11	2.02	0.37	0.49	0.30	7.37	7.29	7.46	15.58	34.63	17.85
	Test 19/4	3.02	5.11	2.07	0.34	0.56	0.34	7.43	7.22	7.42	23.09	32.94	17.96
	Test 19/5	3.38	6.48	2.03	0.42	0.63	0.33	7.39	7.18	7.43	23.09	30.01	21.55
	Test 19/6	4.42	7.68	2.16	0.47	0.82	0.30	7.3	7.04	7.45	18.16	34.79	10.52
	Test 19/7	4.41	8.32	1.96	0.46	0.83	0.32	7.34	7.02	7.41	24.32	31.09	9.89

Table 2: Damage numbers for three selected cross sections, NA indicates that the scan data provided to little data for the analysis in this area.

In general, an increase in the damage numbers is observed with an increasing test duration (see Table 2). The calculated $\bar{S}$ ranging between approx. 0.5 to 8.5 correspond to 5 % to 15 % of displaced armour stones [Rock Manual, 2007]. The revetment condition is classified as 'intermediate damage' [Rock Manual, 2007 ; Hofland et al., 2018]. $\bar{S}$ and $\bar{E}$ are in all but one case slightly larger in *Series 2* than in *Series 1*. This may be due to the different installation: while in *Series 1* the riprap is partly installed by excavator and partly by hand, in *Series 2* the riprap is only packed by hand. $\bar{L}$ is characterised by a large variability. This is likely due to the small distance between the top edge of the slope and still water level as a result of the limited space in the wave basin. Commonly, slopes at inland waterways have a larger freeboard. Therefore, $\bar{L}$ is not considered in the following analyses.

5.2 Correlations and Comparison to Previous Investigations

To evaluate the validity of the obtained experimental results and the applicability of the damage progression model (DDPM) by Castillo et al. (2012) to this experimental data, firstly, the results are compared to experiments by Melby and Kobayashi (1998a, 1998b). The data by Melby and Kobayashi (1998a, 1998b) is used for validation as Castillo et al. (2012) developed their model based on these data.

Although not shown graphically, the herein presented test series confirm the exponential relation between $\bar{S}$ and σ_s found by Melby and Kobayashi (1998a, 1998b). The variability in damage increases with mean damage. The coefficients relating $\bar{E}$ and $\bar{S}$ deviate from the observations by Melby and Kobayashi (1998a, 1998b), see Figure 9a. Although $\bar{E}$ increases with increasing $\bar{S}$, which means that the shape of the eroded area does not change significantly during damage progression, the observed $\bar{E}$ are smaller than those observed by Melby and Kobayashi (1998a, 1998b). In Melby and Kobayashi (1998a, 1998b), $\bar{E}$ initially increases faster than $\bar{S}$. In the herein presented tests, $\bar{E}$ and $\bar{S}$ increase almost linearly. According to Melby and Kobayashi (1998a, 1998b), the damage starts to extend into depth before it extends towards the slope, whereas in this study, the damage spreads evenly in depth and width. Figure 9b confirms the relation $\bar{C} = C_0 - 0.1\ \bar{S}$ by Melby and Kobayashi (1998a, 1998b). Since $C_0 - \bar{C}$ is a different expression of $\bar{E}$, these results may be also interpreted as confirmation of the linear trend in Figure 9a which produces only a slightly smaller R^2 than the exponential relation.

While the investigations by Melby and Kobayashi (1998a, 1998b) were conducted on slopes with a slope inclination of 1:2, the herein presented tests are conducted on a slope with an inclination of 1:3. It seems reasonable that in the case of the new data with the lower slope inclination, the slope edge is eroded first, whereas in the case of the experiments by Melby and Kobayashi (1998a, 1998b) the damage starts to deepen immediately. One reason for the overestimation of $\bar{E}$ in the case of Melby and Kobayashi (1998a, 1998b) could be the technique used to determine the damage profiles: In Melby and Kobayashi (1998a, 1998b) a potentiometer was used which only determined the slope height in a linear profile, but not three-dimensionally like the laser scanner used in this study. Overall, however, it is assumed that the results of Melby and Kobayashi (1998a, 1998b) and the herein presented tests are in good agreement. The data are therefore suitable for the development and calibration of the DDPM for inland waterways.

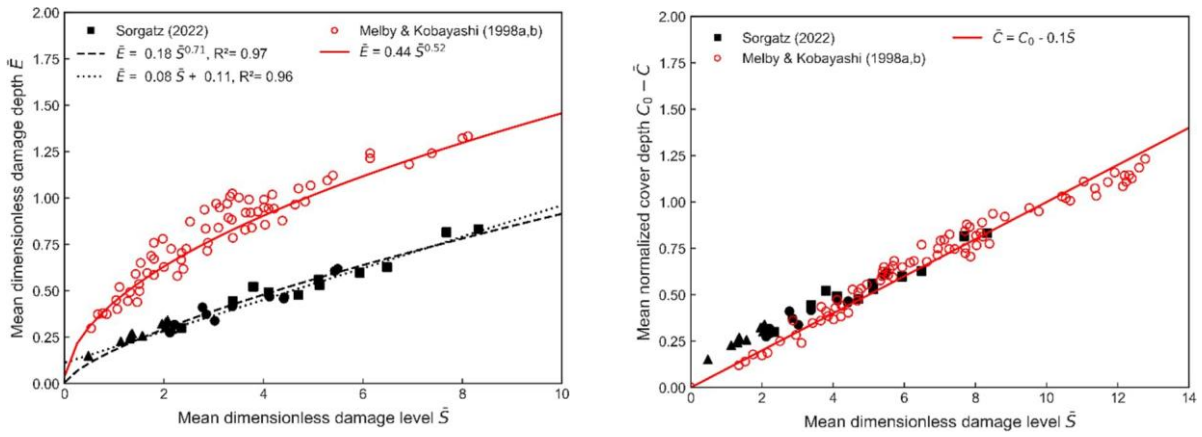

a) Mean dimensionless damage level $\bar{S}$ vs. mean dimensionless damage depth $\bar{E}$

B) Mean dimensionless damage level $\bar{S}$ vs. mean normalised cover depth $C_0 - \bar{C}$

Figure 9: Correlation of different damage indicators and their comparison to the analyses by Melby and Kobayashi (1998a, 1998b)

6 DAMAGE DEVELOPMENT

6.1 Model Calibration

For damage prediction at inland waterways, the DDPM [Castillo et al., 2012] is adapted as it is particularly flexible with regard to the choice of damage indicators and coefficients describing the structure. Furthermore, it reflects the stochastic nature of damage development better than the other models. The model is calibrated for $\bar{S}$ and $\bar{E}$ using the experimental data (see Table 2). To avoid disturbing effects of the walls of the wave basin only data from the central area of the wave basin is used for calibration.

The calibration is conducted as proposed in Campos (2016) and involves two stages (see Figure 10). First, the damage distribution for each group of measurements taken at t^*_i with the median m_e and standard deviation σ_e of the experimental data is determined The results are compared to the theoretical median m_{t_i} and theoretical standard deviation σ_{t_i}, see eq. (10) and eq. (11), to identify suitable *k* and *r* values. For this purpose, $\gamma = 0$ and $b = 0.5$ are fixed as the fitting should be independent of the structures' characteristics; $\mu_0 = 0$ and $\sigma_0 = 0$ [Campos, 2016].

$$m_{t,i} = (\mu_0 + k t_i^*)^b + \gamma \tag{10}$$

$$\sigma_{t,i} = b \sqrt{\frac{\sigma_0^2 + r t_i^*}{(\mu_0 + k t_i^*)^{2-2b}}} \tag{11}$$

Secondly, the damage development is approximated using least squares regression. With the prior knowledge on the relation of wave action and duration, all input parameters are determined via optimisation. The total error over the entire damage development is selected as the optimisation target. For target functions that include local minima, the results of the optimisation process can depend on the provided initial guess. Thus, to identify the global minimum, the starting point is selected randomly by sampling each input parameter from a previously defined

range for 100 optimisation runs. The minimum of these 100 errors is assumed to be the global minimum. Since *b* and *γ* are considered as structure dependent and thus, independent of the damage indicator, the optimisation is supplemented by a parametric study, where *b* and *γ* are kept constant while the other parameters are optimised (see Table 3).

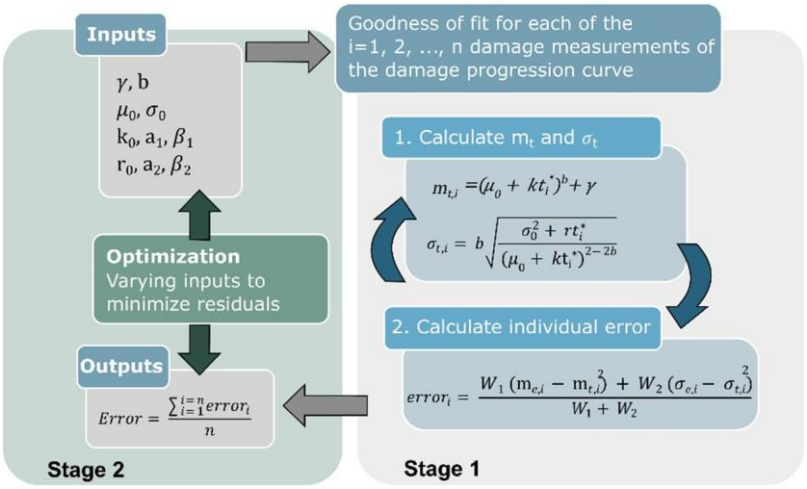

Figure 10: Calibration workflow as proposed by Campos (2016). Varying inputs are achieved through random sampling of the optimisation starting points. Illustration based on Campos (2016).

The first calibration phase confirmed the following exponential relationship between wave action parameters and relative duration found by Campos (2016):

$$k = k_0 + a_1(N_s) \cdot (t^*)^{\beta_1(N_s)} \tag{12}$$

$$r = r_0 + a_2(N_s) \cdot (t^*)^{\beta_2(N_s)} \tag{13}$$

The empirical coefficients $a_{1,2}$ and $\beta_{1,2}$ are a function of N_s. Each interval of constant N_s can be described by the same $a_{1,2}$ and $\beta_{1,2}$.In the herein presented data set, N_s and, thus, $a_{1,2}$ and $\beta_{1,2}$.are constant over the entire study. This approximation corresponds to the situation at artificial inland waterways. The differences between design-relevant wave events are moderate and do not lead to a significant change in N_s. The empirical coefficients k_0 and r_0 are related to the herein investigated wave action. For different load scenarios, they may have to be re-calibrated.

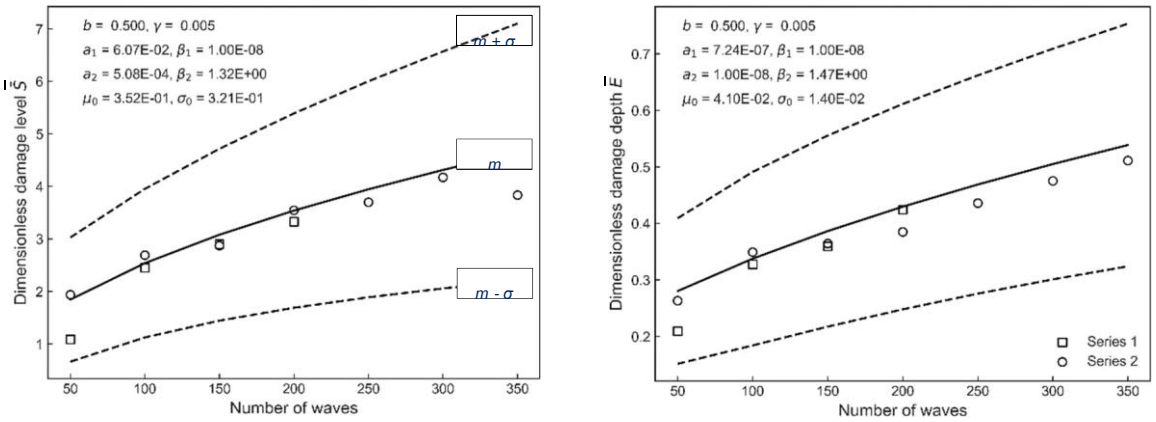

Figure 11: Damage progression of $\bar{S}$ and E as a function of waves. While the solid lines indicate the median m of the damage distributions. The dashed lines represent $m \pm \sigma$.

The results of the second calibration stage (optimisation) are presented in Figure 11 and Table 3. The input parameters μ_0, σ_0, k_0, r_0, a_1, a_2, β_1 and β_2 vary depending on the chosen damage indicator; b = 0.500 and γ = 0.005 are identified as the structure dependent parameters that result in the least total error.

		b	γ	a_1	β_1	a_2	β_2	k_0	r_0	μ_0	σ_0	*Error*
$\bar{S}$	1	0.56	0.285	3.36E-02	4.70E-04	4.25E-05	1.56E+00	5.94E-03	1.74E-01	0.276	0.010	8.23E-02
	2	**0.250**	0.002	5.86E-03	9.25E-01	3.30E-04	2.71E+00	1.00E-08	1.00E+00	0.100	1.000	8.33E-02
	3	**0.500**	0.004	2.38E-02	1.00E-08	1.06E-03	1.20E+00	3.71E-02	2.47E-01	0.320	0.213	8.24E-02
	4	**0.750**	0.401	1.76E-02	6.51E-06	4.92E-07	1.91E+00	1.60E-04	4.50E-02	0.905	1.000	8.45E-02
	5	**1.000**	0.001	9.33E-03	1.00E-08	2.43E-07	1.68E+00	3.76E-05	1.04E-02	1.542	0.954	8.98E-02
	6	**0.250**	**0.005**	5.79E-03	9.27E-01	3.23E-04	1.33E+00	1.00E-08	1.00E+00	0.100	1.000	8.33E-02
	7	**0.500**	**0.005**	6.07E-02	1.00E-08	5.08E-04	1.33E+00	1.70E-08	2.86E-01	0.352	0.321	8.23E-02
	8	**0.750**	**0.005**	1.67E-02	3.46E-05	2.47E-07	2.00E+00	1.63E-03	5.48E-02	1.568	0.981	8.50E-02
	9	**1.000**	**0.005**	1.00E-08	1.00E-08	3.87E-07	1.62E+00	9.21E-03	9.68E-03	1.576	0.995	8.98E-02
$\bar{E}$	1	0.475	0.001	3.32E-04	1.31E-07	7.18E-06	5.00E-01	3.32E-04	1.00E-08	0.035	0.047	7.39E-04
	2	**0.250**	0.001	5.82E-06	5.56E-01	2.41E-07	7.93E-01	4.10E-07	1.00E-08	0.010	0.010	1.32E-03
	3	**0.500**	0.001	6.94E-04	4.93E-04	3.94E-06	6.11E-01	2.01E-08	2.56E-08	0.044	0.062	7.38E-04
	4	**0.750**	0.190	3.39E-04	1.08E-07	3.28E-06	5.00E-01	3.39E-04	4.54E-05	0.010	0.060	7.45E-04
	5	**1.000**	0.038	1.01E-08	1.00E-08	3.68E-06	5.00E-01	8.39E-04	1.80E-05	0.215	0.132	7.81E-04
	6	**0.250**	**0.005**	5.16E-07	1.00E+00	1.49E-07	8.82E-01	4.35E-07	1.00E-08	0.011	0.010	1.39E-03
	7	**0.500**	**0.005**	7.24E-07	1.00E-08	1.00E-08	1.47E+00	6.96E-04	9.35E-05	0.041	0.014	7.31E-04
	8	**0.750**	**0.005**	1.00E-08	5.03E-01	3.70E-06	5.44E-01	8.40E-04	3.56E-05	0.145	0.107	7.61E-04
	9	**1.000**	**0.005**	1.00E-08	1.17E-02	2.93E-06	5.28E-01	8.39E-04	2.23E-05	0.248	0.132	7.81E-04

Table 3: Results of parametric study: Coefficients of the damage progression model based on $\bar{S}$ and $\bar{E}$ determined by optimisation. Bold printed parameters were fixed during optimisation. The grey highlighted row shows the recommended parameter set.

6.2 Modified Model

As for waterways the number of vessels causing damage is significant for damage progression, eq. (10–13) are modified to account for individual vessel passages. From $t^*=tn/T_m$ follows under the assumption of a constant ratio of event duration and mean wave period:

$$t^* = n_{waves} = B^* \cdot n_{vessels} \tag{14}$$

where n_{waves} is the number of waves exceeding the design, B^* represents the proportion of vessels exceeding the limit state from the total numbers of vessels passing the waterway $n_{vessels}$, e.g. per year. Since the number of critical wave events is limited, but depends on the waterway and the desired maintenance, two design scenarios are identified in accordance with the German design standard [GBB, 2010]:

- Case 1: The design case occurs rarely in 1 % of vessels passages, B^* = 0.01
- Case 2: The design case occurs frequently in 5 % of vessels passages, B^* = 0.05

Consequently, the following general relationship for the vessel dependent prediction of damage development at inland waterways is derived:

$$m[D^*(n_{vessels})] = (\mu_0 + kB^* n_{vessels})^b + \gamma \tag{15}$$

$$\sigma\,[D^*(n_{vessels})] = \sqrt{b \cdot \left(\frac{\sigma_0^2 + rB^* n_{vessels}}{\mu_0 + kB^* n_{vessels}}\right)^{2-2\cdot b}} \tag{16}$$

$$k = k_0 + a_1(N_s) \cdot B^* n_{vessels}^{\beta_1(N_s)} \tag{17}$$

$$r = r_0 + a_2(N_s) \cdot B^* n_{vessels}^{\beta_2(N_s)} \tag{18}$$

Figure 12 illustrates the damage progression for the number of passing vessels obtained with eq. (14–18) and the parameter set highlighted in Table 3. It is observed that the progression of $\bar{S}$ for a conserva- tive design (Case 2) is highly uncertain compared to an optimistic design (Case 1) and compared to the progression of $\bar{E}$ (Case 1 and Case 2). The uncertainty in $\bar{S}$ is a result of the variability of the input data; in this case, the experimentally obtained $\bar{S}$. It is assumed that $\bar{S}$ is more difficult to determine by means of the herein proposed analyses method and, thus, characterized by a larger variability ($0.2 < \sigma_S < 1.7$) compared to $\bar{E}$ ($0.06 < \sigma_E < 0.22$). Moreover, as observed in the experimental data, the variability in damage increases with increasing mean damage. Thus, for both, $\bar{S}$ and $\bar{E}$, the prediction uncertainty increases with an increasing number of passing vessels. The 'decline in damage' without maintenance as observed in Figure 12 must be considered as prediction uncertainty without physical meaning regarding the actual revetment condition. It must be noted that, in the case of $\bar{S}$, the large standard deviation results in a limited predictive power of the model with increasing wave number.

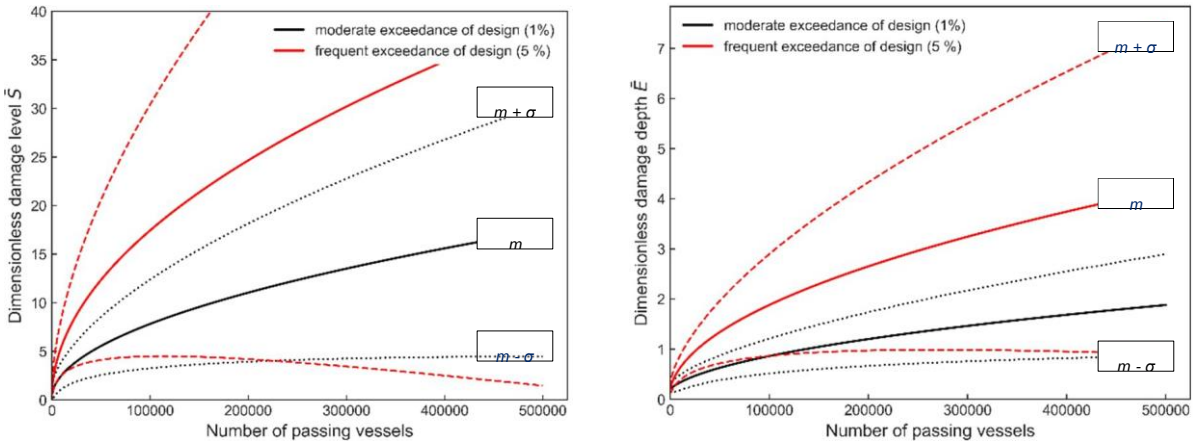

Figure 12: Damage progression of $\bar{S}$ and $\bar{E}$ as a function of the number of passing vessels. While the solid lines indicate the median m of the damage distributions. The dashed lines represent $m \pm \sigma$.

7 DISCUSSION

A ship's passage causes a complex load pattern of waves and currents on the shore of a waterway. Depending on the cross-sectional area, the passing vessels, their geometry and velocity, the mean wave period of a vessel passages ranges between 1 s to 300 s [Almström and Larson, 2020 ; Mahmoudi Kurdistani et al., 2019]. Within the scope of this study, this wide range of wave periods and the complex ship-induced wave pattern are not investigated. However, since short-period waves are the most critical for revetment stability [Melby and Kobayashi, 1998a], it can be assumed that the presented investigations represent a worst case scenario.

If a model is scaled, scale effects occur. These scale effects may not be neglectable in the context of water-shore interactions, as they affect the breaking behaviour of the waves [Kobus, 1984 ; Heller, 2011]. For the herein presented tests, a full-scale embankment model was built. One drawback of this 1:1 scale model is that – indicated by some measurements – turbulent flow conditions and irregular waves may have occurred. It is beyond estimation to what extent these turbulences have an influence on the result. For the analyses and the subsequent calibration of the damage progression model, the wave conditions are described as accurately as possible with the help of redundant measurements. In this way, it is assumed that a good agreement between the experimental data, the new damage progression model and future field observations is achieved. Furthermore, due to cost constraints, the herein presented analyses are based on a limited number of full-scale model tests. It must thus be acknowledged that the

provided model coefficients comprise uncertainty which is only partially included in the variability of the model.

The assessment of damage progression by means of subsequent laser scans shows satisfactory results. The application to the 1:1 scale model, which is located outside and subject to different effects than a model in indoor test facilities, worked well. Since the majority of laser scanners only works above the water level, the proposed scanning procedure is mainly applicable to revetments within the tidal range, whereas it poses a challenge to the assessment of canals with a constant water level. In these cases, L or the movement of the upper edge of the slope may represent a key figure for characterising the severity of the damage. However, this will require further research.

The newly established damage progression model seems to provide a first good estimate of the damage progression for bank revetments at inland waterways subjected to ship-induced wave attack. As a result of the prescribed layer thickness, at German inland waterways failure starts between $E \approx 3 - 4$. The analyses in Section 5.2 show that depending on the design case, this point is reached after more than 240,000 vessel passages in Case 2 or rarely in Case 1. For a below-average dimensioned waterway (Case 2) with approx. 20,000 ships per year, this means that without maintenance, failure will occur after approx. 8-12 years. A well-dimensioned waterway (Case 1), on the other hand, requires hardly any maintenance and has a low probability of failure. These results agree very well with statements from expert interviews [Sorgatz, 2021] and correlations of maintenance measures and revetment stability [Sorgatz and Kayser, 2022].

Finally, let us consider the failure specifications of Rock Manual (2007), Melby and Kobayashi (1998a, 1998b) and Hofland et al. (2018) as summarised in Section 2.3: In the presented test series, $\bar{E} = 0.8$ is reached, whereas $\bar{S} < 12$. Failure is not evident because the existing rather thick armour layer ($C_0 = 7.7\, D_{n50}$) still protects filter layer and soil from erosion. In the case of canal revetments, this layer thickness is a result of additional design specifications such as safety in the event of ship impact, anchor drop and ultraviolet radiation. This brief comparison of recommendations for breakwaters and the findings of this study illustrates that focusing on S may not provide comparable information on failure for different constructions. The failure criterion should be independent of the structures' characteristics. Moreover, S seems to be characterised by a large variability throughout all studies. In future recommendations regarding the stability of riprap structures, the failure criterion S may be supplemented by C or $C_0 - E$ indicating the armour layer thickness still in place. For standardised revetment constructions the increase in E may be a suitable failure criterion. In this case, the damage propagation model calibrated on $\bar{E}$ may assist in scheduling maintenance measures at artificial inland waterways.

8 CONCLUSIONS

In this paper, a riprap revetment is loaded repeatedly with waves. Common damage indicators are evaluated. Based on the experimental data, a damage progression model is modified for the application at artificial inland waterways. For the newly established damage progression model that allows to describe the evolution of two damage indicators over traffic, model coefficients are identified by means of calibration and a parameter study. One of the pending challenges of damage characterization is the standardization of procedures in field and laboratory. The presented analyses contribute to this task by providing a detailed description of the experimental tests and subsequent analyses.

Amongst others, damage progression models aim at predicting failure. In this study, it is concluded that the increase of the mean dimensionless damage depth E may be a suitable failure criterion

for standardised revetment constructions. To compare different structures, C or $C_0 - E$, which indicate the armour layer thickness still in place, may be the most suitable failure criteria. At German inland waterways failure starts at $E \approx 3 - 4$ depending on the armour layer thickness. The damage propagation model calibrated on E^* may assist in scheduling maintenance measures at artificial inland waterways.

Since the herein presented analyses are based on a limited number of model tests, it must be acknowledged that the provided model coefficients comprise uncertainty which is only partially included in the variability of the model. Long-term measurements of vessel passages and damage development on the Dortmund-Ems Canal have started in 2019 and are still ongoing. The results of this study are supposed to assist the further calibration and validation of the damage progression model, for instance, for different load scenarios.

9 ACKNOWLEDGEMENTS

This research was supported by the German Federal Waterways Engineering and Research Institute (BAW), Department Earthworks & Bank Protection. Sincere thanks goes to Dr.-Ing. Jan Kayser, Head of Department Geotechnical Engineering at BAW, for his insightful comments that improved the manuscript significantly. Moreover, the author acknowledges the efforts of Sonja Letzelter who assisted in the experimental tests and their subsequent analyses.

10 NOTATION

Name	Symbol	Unit
Empirical coefficient in damage function	β_1	
Empirical coefficient in damage function	β_2	
Cumulative density function of a standard Gaussian distribution	$\Phi_{(x)}$	
Empirical coefficient describing the structure's topology	γ	
Mean	μ	
Mean of initial damage	μ_0	
Armour stone density	ρ_S	kg/m³
Standard deviation	σ	
Standard deviation of initial damage	σ_0	
Standard deviation of initial cover layer depth	σ_{c_0}	
Experimentally obtained standard deviation of damage indicator	σ_e	
Theoretically obtained standard deviation of damage indicator	σ_t	
Eroded area	A_e	m²
Empirical coefficient in damage function	a_1	
Empirical coefficient in damage function	a_2	
Proportion of vessels exceeding the limit state	B^*	
Normalized cover depth	C	
Initial dimensionless cover layer depth	C_0	
Empirical coefficient describing the structure's characteristics	b	

Name	Symbol	Unit
Cover depth	d_c	m
Maximum slope normal distance between damaged and undamaged profile	d_e	m
Dimensionless damage	D^*	
Mean nominal armour stone diameter	D_{n50}	m
Dimensionless damage depth	E	
Cumulative density function	F	
Significant wave height	H_S	m
Empirical coefficient describing wave action	k	
Empirical coefficient in damage function	k_0	
Hydraulic conductivity	k_f	m/s
Normalised eroded length	L	
Eroded length	l_e	m
Median mass	M_{50}	kg
Median	m	
Experimentally obtained median of damage indicator	m_e	
Theoretically obtained median of damage indicator	m_t	
Number of displaced armour stones within a predefined area	N_d	
Number of displaced armour stone units	N_{od}	
Stability number	N_s	
Time counter	n	
Number of passing vessels	$n_{vessels}$	
Number of waves exceeding the design	n_{waves}	
Empirical coefficient describing wave action	r	
Empirical coefficient in damage function	r_0	
Dimensionless damage level	S	
Mean wave period	T_m	s
Time	t	s
Number of waves	t^*	
Duration time of storm to reach a damage level	t_0	s
Load duration	t_n	s
Width coordinate	X	
Cross-shore coordinate	Y	

10 REFERENCES

Ahrens, J.P. (1970): "The Influence of Breaker Type on Riprap Stability", Paper presented at the 12th Conference on Coastal Engineering, Washington D.C., USA (Coastal Engineering, 12), p. 1557-1566.

Almström, B. and Larson, M. (2020): "Measurements and Analysis of Primary Ship Waves in the Stockholm Archipelago, Sweden", *Journal of Marine Science and Engineering*, 8 (10):743, **https://doi.org/10.3390/jmse8100743**.

Bezuijen, A., Klein Breteler, M. and Bakker, K.J. (1987): "Design Criteria for Placed Block Revetments and Granular Filters", Paper presented at 2nd Copedec, Beijing, China.

Broderick, L. (1983): "Riprap Stability, A Progress Report", Paper presented at Coastal Structures '83, Arlington, Virginia, USA.

Campos, A. (2016): "A Methodology for the Analysis of Damage Progression in Rubble Mound Breakwaters", PhD thesis, Universidad de Castilla-La Mancha, Ciudad Real, Spain.

Castillo, C., Castillo, E., Fernández-Canteli, A., Molina, R. and Gómez, R. (2012): "Stochastic Model for Damage Accumulation in Rubble-Mound Breakwaters Based on Compatibility Conditions and the Central Limit Theorem", *Journal of Waterway, Port, Coastal, and Ocean Engineering*, 138 (6):451–463, **https://doi.org/10.1061/(ASCE)WW.1943-5460.0000146**.

CloudCompare (version 2.11.3) [GPL software] (2018). Retrieved from **https://www.danielgm.net/cc/**.

Daemrich, K.-F., Mathias, H. J. and Zimmermann, C. (1996): "Untersuchungen zur Bemessung von Deckwerken in Schiffahrtskanälen unter Wellenbelastung. Einfluss der Deckschichtdicke auf die Stabilität der Deck- schicht" [Investigations into the design of revetments in shipping channels under wave loads. Influence of the revetment thickness on the stability of the revetment], Paper presented at Wirkungen am Ufer-Befesti- gungen; Wasserbaukolloquium '96, TU Dresden, Dresden, Germany.

DST (2006): "Bericht 1794: Modellversuche zu schiffsinduzierten Wirkungen auf Ufer" [Model tests on ship-in- duced effects on banks], Entwicklungszentrum für Schiffstechnik und Transportsysteme e.V. (unpublished).

Fleischer, P. and Kayser, J. (2006): "BAW-Grundsatzaufgabe. Bestandsaufnahme von Deckwerken. Aufgabenstellung und Struktur. 4. Teilbericht" [BAW Principle Task. Inventory of revetments. Task and structure. 4th report], Bundesanstalt für Wasserbau (ed.).

Font, J.B. (1968): The effect of storm duration on rubble mound breakwater stability. *Coastal Engineering Proceedings*, 1 (11): 2156–1028, **https://doi.org/10.9753/icce.v11.50**.

Font, J.B. (1970): "Damage Functions for a Rubble-Mound Breakwater under the Effect of Swells", *Coastal Engineering Proceedings*, 1(12), **https://doi.org/10.9753/icce.v12.96**.

GBB (2010): "BAWMerkblatt. Grundlagen zur Bemessung von Böschungs- und Sohlensicherungen an Binnen- wasserstraßen" [BAW Code of Practice. Principles for the Design of Bank and Bottom Protection for Inland Waterways], Bundesanstalt für Wasserbau (ed.).

Gier, F. (2017): "Zur Bemessung von verzahnten Setzsteindeckwerken gegen hydrodynamische Belastungen", PhD thesis, RWTH Aachen, Aachen.

Hedar, A. (1965): "Design Of Rock-Fill Breakwaters", American Society of Civil Engineers.

Heller, V. (2011): "Scale Effects in Physical Hydraulic Engineering Models", *Journal of Hydraulic Research*, 49 (3):293-306, **https://doi.org/10.1080/00221686.2011.578914**.

Hofland, B., van Gent, M., Raaijmakers, T. and Liefhebber, F. (2013): "Damage Evaluation Using the Damage Depth", Paper presented at Coastal Structures 2011, Yokohama, Japan.

Hofland, B., Disco, M. and van Gent, M. (2014): "Damage Characterization of Rubble Mound Roundheads", Paper presented at Coastlab14, Application of Physical Modelling to Port and Coastal Protection, Varna, Bulgaria.

Hofland, B., Rosa-Santos, P., Taveira-Pinto, F., de Almeida, E., Lemos, R., Mendonça Conceição, A. and Fortes, J. (2018): "Measuring Damage in Physical Model Tests of Rubble Mounds", Paper presented at Coasts, marine structures and breakwaters. Realising the potential. 11th International Conference, Institution of Civil Engineers, Liverpool, UK, p. 929-940, **https://doi.org/10.1680/cmsb.63174.0929**.

Hudson, R.Y. (1958): "Design of Quarry-Stone Cover Layers for Rubble-Mound Breakwaters", Research Rep. 2-2, U.S. Army Engineer Waterways Experiment Station, Vicksburg, MS.

Hudson, R.Y. (1959): "Laboratory Investigation of Rubble-Mound Breakwaters", Journal of the Waterways and Harbor Division, 85 (WW3):610-659.

Iribarren, R. (1949): "A Formula for the Calculation of Rock-Fill Dikes", Translation from Revista de Obras Publicas, The Bulletin of the Beach Erosion Board, 3 (1):1-15.

Iribarren, R. and Nogales, C. (1951): "Generalization of the Formula for the Calculation of Rock Fill Fikes and Verification of its Coefficients", The Bulletin of the Beach Erosion Board, 5 (1):4-23.

Iribarren, R. and Nogales, C. (1952): "New Confirmation of the Formula for the Calculation of Rock Fill Dikes".

Council on Wave Research (eds.): "Proceedings of the Third Conference on Coastal Engineering", 3rd International Conference on Coastal Engineering, Cambridge, Massachusetts, USA, p. 185-189.

Kayser, J. (2015): "FuE-Abschlussbericht: Entwicklung des Zustands von Deckwerken bei Absenkung des technischen Standards" [Final R&D report: Development of the condition of revetments when the technical standard is lowered], Bundesanstalt für Wasserbau (ed).

Kobus, H. (1984): "Wasserbauliches Versuchswesen" [Hydraulic engineering experiments]. Schriftenreihe des Deutschen Verbandes für Wasserwirtschaft und Kulturbau e.V, 39, Parey, Hamburg.

Köhler, H.J. (1985): "Modellversuche für die Dimensionierung von Deckwerken an Wasserstraßen - Stabilität loser Steinschüttungen" [Model tests for the dimensioning of revetments on waterways - stability of loose rockfills], Mitteilungsblatt der Bundesanstalt für Wasserbau, 56:69-101.

Kreyenschulte, M. (2020): "Wellen-Bauwerks-Interaktion bei mörtelvergossenen Schüttstein-deckwerken" [Wave- structure interaction in mortar grouted riprap revetments], PhD thesis, RWTH Aachen, Aachen.

Lee, D.W., Abt, S.R., Hinkle, N.E., Khattak, M.S., Nelson, J.D., Ruff, J.F., Shaikh, A. and Wittler, R.J. (1987): "Development of Riprap Design Criteria by Riprap Testing in Flumes: Phase I. NU-REG/CR-4651", U.S. Nuclear Regulatory Commission, Washington, D.C., May, 111.

Mahmoudi Kurdistani, S., Tomasicchio, G.R., D'Alessandro, F. and Hassanabadi, L. (2019): "River Bank Protection from Ship-Induced Waves and River Flow", Water Science and Engineering, 12 (2):129-135, **https://doi.org/10.1016/j.wse.2019.05.002**.

MAK (2013): "BAWMerkblatt. Anwendung von Kornfiltern an Bundeswasserstraßen" [BAW Code of Practice.

Bundesanstalt für Wasserbau (ed.): "Application of Grain Filters on Federal Waterways".

MAR (2008): "BAWMerkblatt. Anwendung von Regelbauweisen für Böschungs- und Sohlensicherungen an Bin- nenwasserstraßen" [BAW Code of Practice. Application of standard construction methods for bank and bot- tom protection on inland waterways], Bundesanstalt für Wasserbau (ed.).

Medina, J.R. (1992): "A Robust Armor Design to Face Uncertainties", Coastal Engineering Proceedings, 1 (23), **https://doi.org/10.9753/icce.v23.%25p**.

Melby, J.A. and Kobayashi, N. (1998a): "Progression and Variability of Damage on Rubble Mound Breakwaters".

Journal of Waterway, Port, Coastal, and Ocean Engineering, 124 (6):286-294, **https://doi.org/10.1061/(ASCE)0733-950X(1998)124:6(286)**.

Melby, J.A. and Kobayashi, N. (1998b): "Damage Progression on Breakwaters", Paper presented at the 26th Coastal Engineering Conference (Coastal Engineering, 26), Copenhagen, Denmark, **https://doi.org/10.1061/9780784404119.141**.

Melby, J.A. (1999): "Damage Progression on Rubble-Mound Breakwater", American Society of Civil Engineers (ed.).

Melby, J.A. (2001): "Damage Development on Stone Armored Breakwaters and Revetments", ERDC/CHLCHETN- III-64, US Army Engineer Research and Development Center (ed.).

MMB (2013): "BAWMerkblatt. Materialtransport im Boden" [BAW Code of Practice. Material Transport in Soil], Bundesanstalt für Wasserbau (ed.).

Ouellet, Y. (1972): "Effects of Irregular Wave Trains on Rubble-Mound Breakwaters", Journal of the Waterways and Coastal Engineering Division, 98 (WW1), 1-13, **https://doi.org/10.1061/AWHCAR.0000138**.

PIANC InCom WG 4 (1987): "Guidelines for the Design and Construction of Flexible Revetments Incorporating Geotextiles for Inland Waterways", Supplement to PIANC Bulletin, 57, Permanent International Association of Navigation Congresses.

PIANC MarCom WG 40 (2003): "State-of-the-Art of Designing and Constructing Berm Breakwaters", Permanent International Association of Navigation Congresses.

Pilarczyk, K.W. and den Boer, K. (1983): "Stability and Profile Development of Coarse Materials and their Application in Coastal Engineering", Delft Hydraulics Laboratory, 293.

Pitt, J.D. and Ackers, P. (1983): "Prototype Tests on Riprap under Random Wave Attack", Paper presented at 18th International Conference on Coastal Engineering, Cape Town, Republic of South Africa, **https://doi.org/10.1061/9780872623736.109**.

Rock Manual (2007): "The Rock Manual. The Use of Rock in Hydraulic Engineering", CIRIA, CUR, CETMEF (eds.), London, CIRIA.

Schendel, A., Goseberg, N. and Schlurmann, T. (2016): "Erosion Stability of Wide-Graded Quarry-Stone Material under Unidirectional Current", Waterway, Port, Coastal, Ocean Engineering, 142 (3):04015023-1-04015023-19, **https://doi.org/10.1061/(ASCE)WW.1943-5460.0000321**.

Scotto, M.G., and Guedes-Soares, C. (2007): "Bayesian Inference for Long-Term Prediction of Significant Wave Height", Coastal Engineering, 54 (5):393-340, **https://doi.org/10.1016/j.coastaleng.2006.11.003**.

Shen, Y., Lindenbergh, R., Hofland, B. and Kramer, R. (2017): "Change Analysis of Laser Scans of Laboratory Rock Slopes Subject to Wave Attack Testing", ISPRS Annals of the Photogrammetry, Remote Sensing and Spatial Information Sciences, IV-2 (W4):139-147, **https://doi.org/10.5194/isprs-annals-IV-2-W4-139-2017**.

Sorgatz, J. (2021): "Towards Reliability-Based Bank Revetment Design: Investigation of Limit States and Parameter Uncertainty", Dissertation, RWTH Aachen.

Sorgatz, J., Kayser, J. and Schüttrumpf, H. (2018): "Expert Interviews in Long-Term Damage Analysis for Bottom and Bank Revetments along German Inland Waterways", Paper presented at the 6th International Symposium on Life-Cycle Civil Engineering (IALCCE 2018), Ghent, Belgium.

Sorgatz, J. and Kayser, J. (2022): "Assessment of Maintenance Efforts and Probabilities of Failure at German Inland Waterways to Advance the Design of Bank Revetments", Journal of Coastal and Hydraulic Structures, **https://doi.org/10.48438/jchs.2022.0014**.

Thompson, D.M. and Shuttler, R.M. (1975). *Riprap design for wind-wave attack - A laboratory study in random waves.* Wallingford report EX707 for CIRIA. HR Wallingford (ed.). Hydraulic Engineering Reports.

TLW (2003): "Technische Lieferbedingungen für Wasserbausteine" [Technical delivery conditions for riprap stones], Bundesministerium für Verkehr und Wohnungsbau.

Uliczka, K., Kondziella, B. and Jansch, H. (2018): "FuE-Abschlussbericht. Schiffserzeugte langperiodische Belas- tung zur Bemessung der Deckschichten von Strombauwerken an Seeschifffahrtsstraßen" [R&D Final Report. Ship-generated long-period loading for the design of the revetments of river structures on maritime waterways], Bundesanstalt für Wasserbau (ed.).

USACE (1997): "Design of Coastal Revetments, Seawalls, and Bulkheads", US Army Corps of Engineers.

van de Kreeke, J. (1969): "Damage Function of Rubble-Mound Breakwaters", Journal of the Waterways and Harbor Division, 95 (WW3): 345-354.

van der Meer, J.W. (1987): "Stability of Breakwater Armour Layers – Design Formulae", Coastal Engineering, 11 (3):219-239, **https://doi.org/10.1016/0378-3839(87)90013-5**.

van der Meer, J.W. (1988): "Rock Slopes and Gravel Beaches under Wave Attack", PhD thesis, Delft Hydraulics Laboratory.

van der Meer, J.W. (2000): "Design of Concrete Armour Layers", Presented at the 3rd International Conference on Coastal Structures, Santander, Spain, **http://www.vandermeerconsulting.nl/downloads/stability_c/ 1999_vandermeer.pdf** [accessed: 10.08.2021].

van der Meer, J.W. and Pilarczyk, K.W. (1984): "Stability of Rubble Mound Slopes Under Random Wave Attack", Coastal Engineering Proceedings, 1 (19), **https://doi.org/ 10.9753/icce.v19.176**.

Verheij, H.J. and Bogaerts, M.P. (1989): "Ship Waves and Stability of Armour Layers Protecting Slopes", Paper presented at the 9th International Harbour Congress, Antwerp, Belgium.

Westrich, B., Siebel, R., Vermeer, P. A. and Zwechper, B. (2003): "Neue naturnahe Bauweisen für überströmbare Dämme an dezentralen Hochwasserrückhaltebecken und Erprobung von Erkundungsmethoden zur Beurteilung der Sicherheit von Absperrdämmen. Schlussbericht zum BWPLUS Forschungsprojekt Stuttgart" [New near-natural construction methods for overflowing dams at decentralised flood retention basins and testing of exploration methods for assessing the safety of cut-off dams. Final report on the BWPLUS research project Stuttgart].

SUMMARY

The Federal German Waterways and Shipping Administration (WSV) maintains about 7,300 km inland waterways. To protect the embankments along these waterways against erosion caused by ship-induced waves and currents, they are mainly secured by bank revetments. Under increasing economic and ecological pressures, the WSV increasingly aims for an integral analysis of revetment stability over their entire life cycle. For this purpose, it is essential to understand and predict damage progression. So far, few studies on damage progression exist which are, however, bound to experimental set-ups mainly related to coastal structures. In particular for inland waterways, i.e. for structures subjected to wave heights ranging between 20 cm and 110 cm and armour stone diameters between 60 mm and 250 mm, data on damage development is sparse. This paper aims at providing insights into the damage development of loose riprap revetments at artificial inland waterways. Based on existing damage progression formulae for coastal structures, a model for the prediction of damage progression at inland waterways is developed. For this purpose, a full-scale embankment model is loaded repeatedly with waves. The damage progression is observed with subsequent laser scans. Common damage indicators are determined. To validate the experimental procedure, the thereby obtained results are compared to experimental data from literature. Subsequently, a new damage progression model is developed and calibrated with the new experimental data.

RESUME

L'administration fédérale allemande des voies navigables et de la navigation (WSV) entretient environ 7 300 km de voies navigables intérieures. Pour protéger les berges de ces voies navigables contre l'érosion causée par les vagues et les courants provoqués par les navires, elles sont principalement sécurisées par des revêtements de berges. Soumis à des pressions économiques et écologiques croissantes, le WSV vise de plus en plus une analyse intégrale de la stabilité des revêtements sur l'ensemble de leur cycle de vie. À cette fin, il est essentiel de comprendre et de prévoir la progression des dommages. Jusqu'à présent, il existe peu d'études sur la progression des dommages, qui sont toutefois liées à des dispositifs expérimentaux principalement liés aux structures côtières. En particulier pour les voies navigables intérieures, c'est-à-dire pour les structures soumises à des hauteurs de vagues comprises entre 20 cm et 110 cm et à des diamètres de pierres de blindage compris entre 60 mm et 250 mm, les données sur l'évolution des dommages sont rares. Cet article vise à fournir des informations sur l'évolution des dommages subis par les revêtements en enrochements libres sur les voies navigables artificielles. Sur la base des formules de progression des dommages existantes pour les structures côtières, un modèle de prédiction de la progression des dommages sur les voies navigables intérieures est développé. Pour ce faire, un modèle de remblai à grande échelle est soumis à des charges répétées de vagues. La progression des dommages est observée à l'aide de balayages laser. Les indicateurs communs de dommages sont déterminés. Pour valider la procédure expérimentale, les résultats obtenus sont comparés aux données expérimentales de la littérature. Ensuite, un nouveau modèle de progression de l'endommagement est développé et calibré avec les données de la littérature.

ZUSAMMENFASSUNG

Die Wasser- und Schifffahrtsverwaltung des Bundes (WSV) unterhält rund 7.300 km Binnenwasserstraßen. Zum Schutz der Böschungen entlang dieser Wasserstraßen vor Erosion durch Erosion durch schiffsbedingte Wellen und Strömungen zu schützen, werden sie hauptsächlich durch Uferbefestigungen gesichert. Unter dem zunehmenden ökonomischen und ökologischen Druck strebt die WSV zunehmend eine integrale Analyse der Deckwerksstabilität über den gesamten Lebenszyklus an. Hierfür ist es unerlässlich, den Schadensverlauf zu verstehen und vorherzusagen. Bislang gibt es nur wenige Studien zum Schadensverlauf, die jedoch an Versuchsaufbauten gebunden sind, die sich hauptsächlich auf Küstenbauwerke beziehen. Insbesondere für Binnenwasserstraßen, d. h. für Bauwerke, die Wellenhöhen zwischen 20 cm und 110 cm und Wasserbausteindurchmessern zwischen 60 mm und 250 mm ausgesetzt sind, liegen nur wenige Daten zur Schadensentwicklung vor. Ziel dieser Arbeit ist es, Erkenntnisse über die Schadensentwicklung von losen Deckwerken an künstlichen Binnenwasserstraßen zu gewinnen. Basierend auf bestehenden Schadensverlaufsformeln für Küstenbauwerke wird ein Modell zur Vorhersage des Schadensverlaufs an Binnenwasserstraßen entwickelt. Dazu wird ein Deichmodell in Originalgröße wiederholt mit Wellen belastet. Der Schadensverlauf wird mit anschließenden Laserscans beobachtet. Es werden allgemeine Schadensindikatoren ermittelt. Zur Validierung des experimentellen Verfahrens werden die so gewonnenen Ergebnisse mit experimentellen Daten aus der Literatur verglichen. Anschließend wird ein neues Schadensfortschrittsmodell entwickelt und mit diesem kalibriert.

RESUMEN

La Administración Federal Alemana de Vías Navegables y Navegación (WSV) mantiene unos 7.300 km de vías navegables interiores. Para proteger los diques a lo largo de estas vías navegables contra la erosión causada erosión causada por las olas y las corrientes inducidas por los buques. Debido a las crecientes presiones económicas y ecológicas, la WSV aspira cada vez más a un análisis integral de la estabilidad de los revestimientos a lo largo de todo su ciclo de vida. Para ello, es esencial comprender y predecir la progresión de los daños. Hasta la fecha, existen pocos estudios sobre la progresión de los daños que, sin embargo, se limitan a montajes experimentales relacionados principalmente con estructuras costeras. En particular, para las vías navegables interiores, es decir, para las estructuras sometidas a alturas de ola que oscilan entre 20 cm y 110 cm y a diámetros de piedras de blindaje entre 60 mm y 250 mm, los datos sobre la evolución de los daños son escasos. El objetivo de este artículo es proporcionar información sobre la evolución de los daños en revestimientos de escollera suelta en vías navegables interiores artificiales. Basándose en las fórmulas de progresión de daños existentes para estructuras costeras, se desarrolla un modelo para la predicción de la progresión de daños en vías navegables interiores. Para ello, se carga repetidamente con olas un modelo de terraplén a escala real. La progresión de los daños se observa con escáneres láser posteriores. Se determinan los indicadores comunes de daños. Para validar el procedimiento experimental, los resultados así obtenidos se comparan con datos experimentales de la literatura. Posteriormente, se desarrolla un nuevo modelo de progresión de los daños y se calibra con los datos de la literatura.